T.C.
AYDIN ADNAN MENDERES UNIVERSITY
GRADUATE SCHOOL OF NATURAL AND APPLIED SCIENCES
MASTER'S PROGRAMME IN CIVIL ENGINEERING
2021-YL-028

SEISMIC COLLAPSE CAPACITY OF BRICK INFILLED REINFORCED CONCRETE FRAMES WITH OPEN GROUND STORY

EMAD KANAS
MASTER'S THESIS

SUPERVISOR
Assoc. Prof. Dr. Emre AKIN

This thesis was supported by Aydın Adnan Menderes University Scientific Research Projects Unit (Project number MF-19013)

AYDIN–2021

ACKNOWLEDGEMENT

I truly wish to express my heartfelt thanks to my supervisor Assoc. Prof. Dr. Emre AKIN for his patience, support and professional guidance throughout this thesis project. Without his encouragement and guidance the study would not have been completed.

I would like to send my special appreciation and thanks to my father Mostafa and my mother Nadrah for their direct and indirect motivation and supporting to complete my master degree.

TABLE OF CONTENTS

LIST OF ABBREVIATIONS

ASCE : American Society of Civil Engineers

BF : Bare Frame

CCSM : Collapse Capacity Spectrum Method

CP : Collapse Prevention

DL : Dead Load

ESDOF : Equivalent Single Degree of Freedom

FEMA 350: Federal Emergency Management Agency

GML : Ground Motion Level

IDA : Incremental Dynamic Analysis

IM : Intensity Measure

LL : Live Load

MDOF : Multi Degree of Freedom

NC : Near Collapse

NPD-BF : Bare Frame Without P-Delta Effect

NPD-OGS : Open Ground Story Frame Without P-Delta Effect

OGS : Open Ground Story

PBEE : Performance-Based Earthquake Engineering

PD-BF : Bare Frame With P-Delta Effect

P-Delta : Destabilizing Effect of Gravity Loads

PD-OGS : Open Ground Story Frame With P-Delta Effect

PEER : Pacific Earthquake Engineering Research Center

RC : Reinforced Concrete

SD : Significant Damage

SDOF : Single Degree of Freedom

SPO : Non-Linear Static Pushover

TEC : Turkish Earthquake Code

LIST OF SYMBOLS

$f_{m'}$: Compressive strength of infill walls

E_m : Modulus of elasticity of infill walls

f_{ws} : Shear resistance of mortar

f_{wu} : Sliding resistance

σv : Vertical compression stress

h : Story height

t_{inf} : Thickness of infill panels

h_{inf} : Height of infill walls

E_c : Modulus of elasticity for concrete

I_c : Moment of inertia of the column

θ : Angle of inclination of the diagonal of infill wall

b_w : Strut width

d_w : Diagonal length of infill wall

μ : Friction coefficient of shear spring

τ_{max} : Maximum shear resistance

τ_o : Shear bond strength

R_{RUP} : Rupture distance

R_{JB} : Joyner-Boore Distance

V_{s30} : Shear wave velocity over the top 30 m of subsurface

Φ : Mode shape vector

M_1 : Generalized mass

L_1, Γ_1 : Modal properties

M_1^* : Base shear effective modal mass

T_1 : Fundamental period

m_j : Mass of the “j”th story at the fundamental mode

Φ_{j1} : Modal displacement of the “j”th story at the fundamental mode

T_A : lower limit corner periods of the constant acceleration zone of the design spectrum

T_B : upper limit corner periods of the constant acceleration zone of the design spectrum

V_b : Base shear

δ_{roof} : Roof drift

S_a : Spectral acceleration

S_d : Spectral displacement

Φ_{N1} : Modal displacement of the roof level at the fundamental mode of vibration

$S_{d,inelastic}$: Inelastic displacement demands

$S_{d,elastic}$: Elastic displacement demands

α_s : Global hardening ratio

θ_e : Elastic stability coefficient

θ_i : Inelastic stability coefficient

V_y : No P-delta base shear corresponding to idealized yield point

X_{Ny} : Displacement corresponding to idealized yield point

T_a : Period of the auxiliary ESDOF system

θ_a : Auxiliary stability coefficient

m_i : Mass of the «i»th story

N : Number of stories

ϕ_i : «i»th Story element of the mode shape vector for the fundemantal mode

CC_d : Collapse capacity

λ_{MDOF} : Transformation factor

CC_{MDOF} : Collapse capacity of the actual multi degree of freedom system

CC_{ESDOF}: Collapse capacity of the Equivalent Single Degree of Freedom system

V_{Py} : Yield base shear force with P-delta

K_s : Effective stiffness

θ_a-a_s : Post-yield stiffness ratio

V : Max base shear

M : Total mass

γ_{el} : Primary and secondary seismic elements

α : Confinement effectiveness factor

l_o : Lap length

d_{bL} : Bar diameter

ε_c : Concrete strain

LIST OF FIGURES

LIST OF TABLES

ÖZET

ZEMİN KATI AÇIK TUĞLA DOLGU DUVARLI BETONARME ÇERÇEVELERDE SİSMİK GÖÇME KAPASİTESİ

Kanas E. Aydın Adnan Menderes Üniversitesi, Fen Bilimleri Enstitüsü, Mühendislik Programı, Yüksek Lisans Tezi, Aydın, 2021.

Amaç: Bu çalışmada, deprem yer hareketi nedeniyle zayıf betonarme çerçeve türü yapılardaki göçme kapasitesinin değerlendirilmesi konu edilmektedir.

Materyal ve Yöntem: Bu amaçla belirlenen bir bölgede bulunan dolgu duvarsız boş çerçeve (BÇ) ve açık zemin katlı, bir başka ifadeyle zemin katı boş, üst katlar dolgu duvarlı çerçeve (AZKÇ) olacak şekilde betonarme çerçeve seçilmiştir. Beş katlı bu betonarme çerçeveler P-Delta etkilerini dikkate alarak ve almayarak iki farklı şekilde analiz edilmişlerdir. Modal analiz, statik itme analizi ve 11 adet yer hareketi ivme kaydı kullanılarak artımsal dinamik analiz gerçekleştirilmiştir. Yer hareketi ivme kayıtları Aydın'da bir koordinat için oluşturulan deprem senaryosuna uygun olarak seçilmiştir. Tüm analizler "Seismostruct 2020" yazılımı kullanılarak gerçekleştirilmiştir.

Bulgular: Modellerin göçme kapasitesini pratik olarak hesaplamak amacıyla, eşdeğer tek serbestlik dereceli sistemlerin itme analiz sonuçlarına dayanan göçme kapatesi spektrumu yönteminden faydalanılmıştır. Ayrıca, güncel Türkiye Bina Deprem Yönetmeliği'ne uygun olarak doğrusal olmayan performans değerlendirmesi gerçekleştirilmiştir. BÇ ve AZKÇ modellerinin göçme kapasitelerindeki değişiklikler P-Delta etkileri dikkate alınarak değerlendirilmiştir. Farklı deprem yönetmeliklerinde göçme kapasitesi için verilen limit durum tanımları artımsal dinamik analiz sonuçları kullanılarak değerlendirilmiştir. İlave olarak, artımsal dinamik analiz ve göçme kapasitesi sonuçları karşılaştırılmıştır.

Sonuç: Sonuçlara bakarak, artımsal dinamik analiz sonuçlarıyla karşılaştırıldığında göçme kapasitesi spektrumu yönteminin göçme kapasitesini daha büyük olarak hesapladığı söylenebilir. Ayrıca, özellikle açık zemin katlı dolgu duvarlı betonarme çerçevelerde göçme kapasitesi limit durumu için yeni bir tanım yapılması gerektiği söylenebilir.

Anahtar kelimeler: Göçme kapasitesi spektrumu yöntemi; Göçme kapasitesi; Artımsal dinamik analiz; Eğilme Dayanımlı Çerçeve; Açık zemin kat; P-delta etkisi.

ABSTRACT

SEISMIC COLLAPSE CAPACITY OF BRICK INFILLED REINFORCED CONCRETE FRAMES WITH OPEN GROUND STORY

Kanas E. Aydın Adnan Menderes University, Graduate School of Natural and Applied Sciences, Civil Engineering Program, Master Thesis, Aydın, 2021.

Objective: In this study, the evaluation of the collapse capacity due to earthquake excitation is discussed for regular non-ductile reinforced concrete (RC) frame structures.

Material and Methods: For this aim, a particular location and a reinforced concrete frame model with two different infill patterns, bare frame (BF) and open ground story (OGS) have been chosen. In this research, five-story reinforced concrete frame models were analyzed either with or without P-delta effect. Eigenvalue analyses, static pushover analyses, and incremental dynamic analysis (IDA) for 11 ground motion records were utilized. The ground motion records were selected by considering an earthquake scenario for the selected coordinates in Aydın. All the analyses were performed using "Seismostruct 2020" software package.

Results: The collapse capacity spectrum method which uses the equivalent single degree of freedom (ESDOF) systems based on pushover analysis results was performed to practically determine the collapse capacity of the models. Besides, the nonlinear seismic assessment of the models according to the latest Turkish Earthquake Code was conducted. The change in the collapse capacity in the case of BF and OGS models with a consideration of P-delta effects were evaluated. The collapse limit state definitions of various seismic codes were assessed by using the IDA results. Additionally, the results obtained from IDA and collapse capacity spectrum methods were compared.

Conclusion: From the outcomes, it can be concluded that the collapse capacity spectrum method over-estimates the collapse capacity significantly when we compare with the results of incremental dynamic analysis. Besides, it may be stated that a new collapse limit state definition is required especially for the reinforced concrete frames with OGS.

Keywords: Collapse capacity spectrum method; Global collapse capacity; Incremental dynamic analysis; Moment-resisting frame; P-delta effect.

1. INTRODUCTION

1.1. Background

Earthquake is one of the most harmful natural hazards. Earthquakes do not destroy the settlement area only, but they may also destabilize the economy and social structure of the economy. Earthquakes occur several times a day in different locations of the world. Major earthquakes occur most frequently in particular areas of the earth's surface that are called seismic hazard zones. The enormous damage in these previous earthquakes that was determined by site-survey studies has revealed the seismic vulnerability of existing buildings (Adam et al., 2004; Bernal, 1998; Ibarra and Krawinkler, 2005). Most of these buildings were designed either according to the past seismic design codes under insufficient regulations and/or constructed without supervision. In order to prevent catastrophic damage in future earthquakes, large-scale urban renewal work has been performed in Turkey. Yet, it is clear that a huge building stock in the seismically active zones still requires performance assessment with regards to the current seismic code regulations (TEC, 2019).

For reinforced concrete (RC) buildings, inappropriate design including deficiencies such as soft and weak stories, torsional irregularity, weak column-strong beam, and short column has a potential to cause significant problems during a major earthquake. The use of poor concrete, plain smooth bars, and improper reinforcement detailing may also lead to substantial damage. Besides, the irregular distributions of strength and stiffness either along with the building height or in the plane of the story that may be caused by the non-uniform and asymmetric positioning of infill walls may provoke unfavorable damage in the structural system. In addition to this, improper workmanship, absence of engineering services, and construction with inadequate detailing of the structural elements requirement are other reasons for damage.

The effects of masonry infill partitions on the seismic response and interaction of these members with the surrounding frame depend on many variables which are not straightforward to identify. Despite the level of knowledge about the infill walls, these members have generally been treated as non-structural members by the seismic codes. And their effects on the seismic response have been considered indirectly only in certain parts of the code regulations, such as ultimate lateral drift ratio control. Any model to represent these members in the seismic design

or assessment has not been suggested in the design codes. Therefore, the effect of the irregular distribution of infill walls on the deficiencies such as «soft-story» cannot be considered. When the rigidity of one story is lower compared to the other stories, an accumulation of seismic demands at that particular story is observed and described as «soft-story». The soft-story may be induced by the open ground story (OGS) where the infill walls are absent only at the ground story to use those areas for car parking or commercial services.

It is well-known fact that the infill walls result in a significant increase in lateral rigidity and strength of reinforced concrete (RC) frames. The irregular distribution of these members may lead to non-uniform allocation of this excessive stiffness/strength and accordingly a possible structural deficiency. When the structure is pushed into highly nonlinear behavior under strong ground motions, the local failure of infills may also cause unexpected shear damage of the columns (i.e. captive column effect) (Dolšek & Fajfar, 2001; Negro & Colombo, 1997).

P-delta or in other words, the destabilizing effect of gravity loads, is defined as additional demands on the vertical members described as second order moments as illustrated in Fig. 1.1.

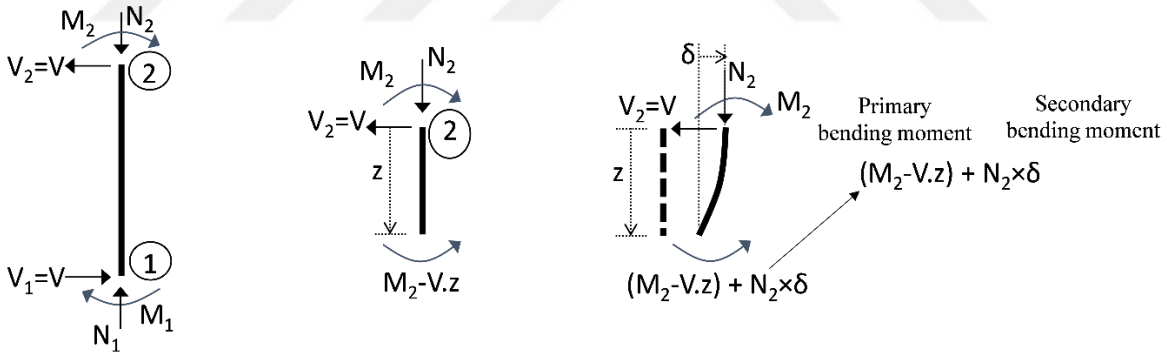

(a) Internal forces at the members ends obtained from a linear structural analysis

(b) The bending moment at a «z» distance from end «2» (from linear structural analysis)

(c) The bending moment at a «z» distance from end «2» when there occurs a relative lateral drift (δ) between these two sections (highly nonlinear inelastic response).

Figure 1.1. Definition for P-Delta effect for vertical member

The code regulations denote that the pushover capacity curve can have a negative post-peak slope (in the highly inelastic range of response) due to second order effects. Pushover

analysis is not allowed in that case and time history analysis is suggested for seismic performance assessment of an existing structure. P-delta effects may cause additional seismic demands and even lead to the collapse of the building. This is especially true for the cases when the structure is pushed into a highly inelastic response (i.e. high ductility demand).

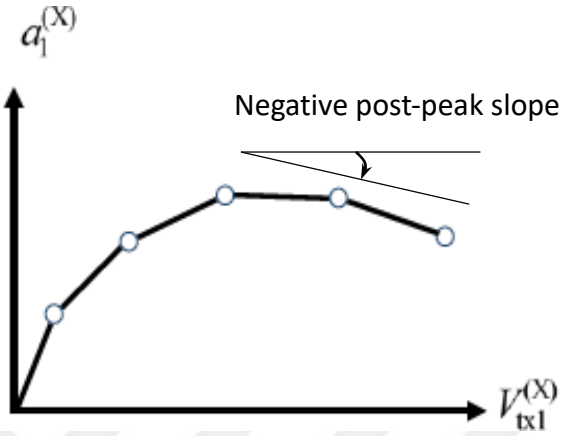

Figure 1.2. Negative post-peak slope for force-displacement curve with P-Delta effect

The prediction of collapse capacity of structural systems subjected to seismic excitation with high confidence is one of the main objectives of earthquake engineering. Despite the fact that increased research efforts in recent years led to a greater understanding of global collapse and some processes behind it, assessment of seismic collapse is still a challenging task. Besides, the approach should include the P-Delta effects on the global collapse of the structural systems.

1.2. Motivation of the Study

This study attempts to evaluate the limit for the collapse in the case of reinforced concrete (RC) bare frame (BF) and open ground story (OGS) frame structures which are vulnerable to the global P-delta effect. The motivation of the study may be explained as follows:

- The columns at the ground story are more sensitive to the P-delta effects since the axial load and inter-story drifts are generally highest in this particular story.
- Additionally, when the ground stories are planned to be open without infill walls (OGS), this story (actually columns of this story) will have less stiffness compared to the upper stories which may further increase the inter-story drifts and resulting sensitivity of ground story columns against P-delta effects.

- Due to these reasons, the collapse may be triggered earlier due to P-delta effects at the OGS which is aimed to be determined by this study.
- Besides, the collapse capacity spectrum method (CCSM) which claims to estimate the collapse capacity practically by using the static pushover analysis results has never been assessed for the open ground story RC frame structures.
- The damage limit states defined by different seismic design codes for the assessment of the existing buildings do not consider the existence of infill walls and consequently any irregularity due to the absence of infill walls at a particular study. Therefore, these damage limit state definitions should be assessed for such structures with OGS which are quite prevalent in all the world.

1.3. Objective of the Study

The initial objective of this study is to obtain the tendency of increased P-delta effects in terms of resulting early collapse of the building with irregular distribution of infill walls (open ground story). In order to achieve the essential aim of this study, the following objectives will be achieved:

- Both of collapse capacity spectrum method and incremental dynamic analysis (IDA) will be performed to obtain the collapse capacities of various frame models.
- The convenience of the simplified CCSM proposed by Adam and Jager (2012) will be verified to obtain the collapse capacity of nonductile RC buildings with the open ground story.
- The change in the collapse capacity in the cases of BF and OGS models will be evaluated with a consideration of P-delta effects.
- Certain suggestions may be presented for a more proper seismic assessment of existing buildings with/without OGS according to the code regulations as a result of this study.

2. LITERATURE SURVEY

2.1. Overview

Several studies related to the prediction and evaluation of collapse capacity are readily available. Since the past decade, many papers and academic research works have been published. The following is a summary of some salient studies.

Bernal (1998) carried out the instability of buildings during seismic response depends on a characterization of the instability limit state depending on the reduction of a multi-story building structure to an equivalent SDOF system. It was noted that the likelihood of the global collapse is highly related to the shape of the mechanism that controls the critical displacement cycle and that this shape can be reasonably obtained using a pushover analysis with an appropriately selected lateral load distribution.

Vamvatsikos and Cornell (2002) have presented the seismic performance, capacity, and reliability of structures as seen through incremental dynamic analysis (IDA). They showed that IDA has proved a useful tool, and can be part of both the short and long-term future of Performance-Based Earthquake Engineering (PBEE). Although, it helps quantify the seismic performance of structures, and in the form of the summarized IDA curves and the Intensity Measure IM-capacities it provides a remarkably useful foundation to develop important intuition and create new approaches to PBEE.

Adam, Ibarra, & Krawinkler (2004) have been presented an evaluation of P-delta effects in non-deteriorating MDOF structures from equivalent SDOF systems. The procedure is assessed for different multi-story (RC) frame building structures. The collapse capacity of these structures is obtained from a set of incremental time history dynamic analysis studies including 40 ground motion records whose intensity is gradually increased until P-Delta instability takes place. They detected that the application of the proposed ESDOF systems is appropriate to estimate P-Delta effects in non-deteriorating regular MDOF structures. However, the dispersion of the results decreases as the effect of P-Delta on the nonlinear response increases.

Kadaş (2006) studied the influence of idealized pushover curves on the seismic response, a comprehensive research has been undertaken to evaluate the influence of several existing alternatives used for approximating the capacity curve on seismic demands. Several frames

were tested under a set of 100 ground motion records. Kadaş (2006) conducted nonlinear incremental time history analyses on multi-degree-of-freedom frame systems and nonlinear static pushover analyses were also utilized to obtain the global response of the selected frames. Based on the interpretations made over the comparisons of simplified analysis results with 'exact' results, it was found that no method seems to be clearly superior in all cases at predicting the exact seismic response parameters in terms of roof displacement, maximum inter-story drift and base shear force. However, all methods generally estimated the seismic demand parameters with 20 percent mean error.

Adam, & Jäger (2012) investigated the prediction of the global collapse capacity of earthquake excited regular moment-resisting frame structures which are vulnerable to P-delta effects. They performed a simplified collapse assessment methodology depending on pushover analyses, equivalent single-degree-of-freedom systems, and a collapse capacity spectrum method for several types of frame structures covering a wide range of structural parameters. Then, the global collapse capacity of these structures derived with this methodology and with the computationally expensive incremental dynamic analysis procedure is set in contrast. It was concluded that in the initial design process the collapse capacity spectrum methodology is an efficient tool to evaluate reliably the median and the dispersion of global collapse capacity of P-delta effect regular moment-resisting frame structures subjected to strong earthquake excitation.

Adam and Jäger (2012) investigated the global collapse capacity of earthquake-excited inelastic nondeteriorating SDOF frame systems, which are subjected to the destabilizing effect of gravity loads (second-order effect P-delta). The collapse capacity of the system subjected to a ground motion has been defined as spectral acceleration at its initial structural period, at which the structure becomes unstable. Moreover, median and percentile collapse capacities are plotted against the fundamental period of vibration of structure obtaining the collapse capacity spectra. Nonlinear analyses were applied to acquire the analytical expressions of the design global collapse capacity spectra and collapse capacity fragility curves. From the outcomes of the study, it can be concluded that for the considered type of structures a quick and yet accurate assessment of the relative collapse capacity can be achieved from design collapse capacity spectra, which are presented as functions of the initial period, negative post-yield stiffness ratio, viscous damping and hysteretic loop.

Burgueño, Rigoberto, et al (2016) examined the second-order effects on seismic response of slender bridge columns through an experimental investigation. Two large-scale RC columns

with a relative ratio (shear span to the width of the section) of 12 were evaluated under quasi-static cyclic loading. The destabilizing effect of gravity loads P-delta and the presence of P-δ to the increase of the plastic region were experimentally assessed by comparing primary and secondary moment gradients. It was confirmed the destabilizing second-order effect of gravity loads P-delta demands and showed that the geometric second-order effects of P-δ caused a crucial increase in the extent of the plastic region (Lpr).

In conclusion, although there is a large number of research studies on the topic, the alteration of collapse capacity of an open ground story RC frame with a consideration of P-delta effects for varying fundamental periods has never been evaluated. Therefore, this study which may provide information about the vulnerability of especially OGS frames under P-delta effects.

3. DESCRIPTION OF PROTOTYPE STRUCTURE AND GROUND MOTIONS

3.1. General

Two reinforced concrete frames and a total of 11 ground motions were employed in this study to evaluate the change in the collapse capacity with consideration of P-delta effects on the seismic response of frame structures. The mid-rise frame used in this study contains five stories and two bays. The frame was one of those used by Kadaş (2006), where it was mentioned to be selected from an existing building located in the city of Bursa in Turkey. The dimensions and reinforcement details of the members were slightly changed to obtain non-ductile structural characteristics (Section 3.2). A nonlinear model of the frame was generated by using Seismostruct (2020) software (Section 3.3). The modeling of infill walls for the OGS frames is explained in Section 3.4. Ground motion records were selected for the incremental dynamic analyses (Section 3.5). These records were obtained from the Pacific Earthquake Engineering Research Center (PEER) "NGA-West 2" database by considering an earthquake scenario for the selected coordinates in Aydın.

3.2. Properties of RC Frame

The compressive strength of concrete was considered as 15 MPa, and the characteristic yield tensile strength of both longitudinal and transverse reinforcement was 220 MPa. The number of legs of the transverse reinforcements was two along with both sectional directions. The initial elastic modulus and strain hardening ratio of the steel were assumed as 2×10^5 MPa and 0.005 respectively. The dimensions and reinforcement of beams and columns are shown in Table 3.1. The rigid diaphragms were assumed at the story levels. The uniformly distributed dead and live loads on all the beams, except those at the roof level, were 12.36 kN/m and 0.98 kN/m, respectively. The dead and live loads of the last story beams were 9.62 kN/m and 0.49 kN/m, respectively. The self-weight of the members was taken into consideration with a unit weight of 24 kN/m^3 for the concrete. The unit weight of the infill walls was assumed as 8 kN/m^3 in the OGS models.

Table 3.1. Details of the reinforced concrete members

Section	Dimensions (mm × mm)	Longitudinal Reinforcement	Transverse Reinforcement
Column	500 × 500	10ϕ18	ϕ8/200 mm
Beam-Support	250 × 600	6ϕ18 (top) 4ϕ18 (bottom)	ϕ8/200 mm
Beam-Span		4ϕ18 (top) 6ϕ18 (bottom)	ϕ8/200 mm

3.3. Modeling of RC Frame

The total height of the frame above the ground level considered for the study is 15 m. In the present study, reinforced concrete frame with five stories (ground +4) having a height of 3 m for each story. The typical 5.7 m bay length, two-span planar RC frame has been considered as shown in Figure 3.1. The modulus of elasticity of concrete was estimated as 18200 MPa in accordance with ACI Committee 318 (2008). The tensile strength of concrete was assumed as 1.5 MPa corresponding to 10 percent of the compressive strength. The strain at the peak compressive stress of concrete was considered as 0.002. A uniaxial steel model was utilized for the reinforcement. The beam-column connections were assumed as rigid and the supports at the foundation level were considered as fixed. Distributed inelasticity model provided by Seismostruct (2020) software (with force-based finite element formulations) where the members were divided into four integration sections were utilized for the nonlinear modeling of the columns and beams. The concrete sections were meshed into 100~150 fibers where the number of meshing was determined with regard to both accuracy and convergence problems. The beam-support sectional properties shown in Table 3.1 are assigned to the first and last integration sections of the beams. The beam-span sectional properties are defined for the remaining two integration sections.

Four types of RC frames have been modelled and analyzed in this study, Identifying them according to the consideration of P-Delta effects, namely:

1) Five-story bare frame with P-Delta effect (PD-BF)
2) Five-story bare frame without P-Delta effect (NPD-BF)
3) Five-story open ground story frame with P-Delta effect (PD-OGS)
4) Five-story open ground story frame without P-Delta effect (NPD-OGS)

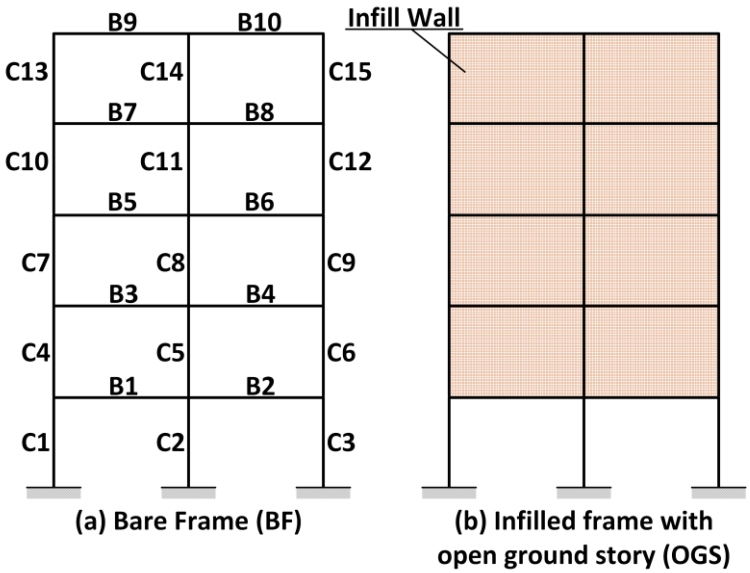

Figure 3.1. Illustrations of RC frame models

3.4. Modeling of Infill Walls

The previously determined infill wall model utilized by Akın (2019), was endorsed for this study. Fair (i.e. average) quality masonry wall properties as stated in FEMA 365 (ASCE, 2000), were brought into application to define the mechanical characteristics of infill walls. The associated compressive strength ($f_{m'}$), modulus of elasticity (E_m) and shear strength of infill walls are 4.1 MPa, 2255 MPa and 0.14 MPa, respectively. The nonlinear modeling of infill walls was provided in accordance with four-node inelastic infill panel element of SeismoStruct (2020). The infill panels consist of two axial struts and one shear strut (only active in compression) along each diagonal direction. The axial strut elements can either be subjected to compression or tension in definition. Nevertheless, in the model, zero was set to be the value of the tensile strength of these elements. The diagonal capacity of axial struts is determined by using the four failure mechanisms. Eqs. (3.1)–(3.4) illustrate the related expressions in correspondence to diagonal tension, sliding of bed joints, corner crushing and diagonal cracking at the center of panel, respectively. For these four failure modes the minimum value calculated is assigned as the axial capacity of struts according to Akın (2019).

$$f_{m\theta} = [0.6f_{ws} + 0.3\sigma_v]/[b_w \,/\, d_w] \tag{3.1}$$

$$f_{m\theta} = [(1.2\sin\theta + 0.45\cos\theta)f_{wu} + 0.3\sigma_v]/[b_w \,/\, d_w] \tag{3.2}$$

$$f_{m\theta} = [1.12 f_{m'} \sin\theta \cos\theta]/[K_1(\lambda h)^{-0.12} + K_2(\lambda h)^{0.88}] \quad (3.3)$$

$$f_{m\theta} = [1.16 f_{m'} \tan\theta]/[K_1 + K_2 \times \lambda h] \quad (3.4)$$

In these equations, f_{ws} and f_{wu} correspond to the shear resistance of mortar joints under diagonal compression and sliding resistance, respectively. The previously defined shear strength (i.e. 0.14 MPa) is assumed for both parameters which may be considered as conservative. The vertical compression stress caused by the gravity forces which was ignored in the model is denoted by σ_v. h is the story height and λ was estimated by Eq. (3.5).

$$\lambda = [(E_m t_{\text{inf.}} \sin 2\theta)/(4E_c I_c h_{\text{inf.}})]^{0.25} \quad (3.5)$$

The thickness of infill panels which was considered as 200 mm as an exterior partition wall is assigned for t_{inf}. The height of infill walls (same as story height) is denoted by h_{inf}. E_c and I_c are the modulus of elasticity for concrete and moment of inertia of the column, respectively. The symbol for the angle which defines inclination of the diagonal of infill with respect to the horizontal axis is θ. The stiffness of the infill panel is defined by the strut width, b_w in Eq. (3.6) where d_w is the diagonal length of infill wall. K_1 and K_2 are defined depending on λh in Eqs. (3.7)–(3.9).

$$b_w = 0.175\,(\lambda h)^{-0.4} \times d_w \quad (3.6)$$

$$K_1 = 1.3 \quad and \quad K_2 = -0.178 \qquad for\ (\lambda h < 3.14) \quad (3.7)$$

$$K_1 = 0.707 \quad and \quad K_2 = 0.01 \qquad for\ (3.14 \leq \lambda h \leq 7.85) \quad (3.8)$$

$$K_1 = 0.47 \quad and \quad K_2 = 0.04 \qquad for\ (\lambda h > 7.85) \quad (3.9)$$

The strain that corresponds to the peak strength of compression struts was assumed to be 0.001 while the ultimate strain of compression struts was assumed to be 0.01. The friction coefficient (μ) of shear spring was set to be 0.7.

According to the manual of SeismoStruct, the expression that was utilized to determine the maximum shear resistance (τ_{max}) is given in Eq. (3.10).

$$\tau_{max} = \tau_0 + 0.30 \quad (3.10)$$

The shear bond strength (τ_o) assumed as equal to the shear strength of infill walls.

3.5. Selected Ground Motions

For incremental dynamic analysis (IDA) of the case study frames, 11 individual ground motions were used in this study. The earthquake excitations recorded at various sites were selected from «Pacific Earthquake Engineering Research Center (PEER)» "NGA-West 2" database in conformity with an earthquake scenario chosen for the selected coordinates in Aydın. Table 3.2 summarizes the parameters considered for the earthquake scenario. The intervals or properties for these parameters were determined considering the historical records and existing faults for the selected location. The selected ground acceleration records were Imperial Valley-02 (1940), Parkfield (1966), Superstition Hills-02 (1987), Erzincan (1992), Landers (1992), Kobe-Japan (1995), Kocaeli-Turkey (1999), Duzce-Turkey (1999), Tottori-Japan (2000), Sierra-Mexico (2010), Darfield-New Zealand (2010). The important features of these ground motions are given in Table 3.3.

Table 3.2. Parameters of the earthquake scenario

Parameter	**Interval/Propert**
Soil class	ZC
Ground motion level (GML)	DD2
Fault Type	Strike-Slip
Earthquake Magnitude	6.0-7.8
Rupture Distance (R_{RUP}) (km)	0-100
Joyner-Boore Distance (R_{JB}) (km)	0-30
Shear Wave Velocity over the top 30 m of subsurface (V_{s30})	100-400

Table 3.3. List of selected ground motions

#	Scale Factor	Intensity (m/sec)	Earthquake Name	Year	Magnitude	Mechanism	Rjb (km)	Rrup (km)	Vs30 (m/sec)
1	1.9469	1.6	Imperial Valley-02	1940	6.95	strike slip	6.09	6.09	213.44
2	1.6186	0.9	Parkfield	1966	6.19	strike slip	9.58	9.58	289.56
3	2.0075	1.1	Superstition Hills-02	1987	6.54	strike slip	18.2	18.2	192.05
4	1.9766	1.8	Erzican_ Turkey	1992	6.69	strike slip	0	4.38	352.05
5	1.7545	2.2	Landers	1992	7.28	strike slip	19.74	19.74	352.98
6	2.502	2	Kobe_ Japan	1995	6.9	strike slip	11.34	11.34	256
7	2.6532	1.3	Kocaeli_ Turkey	1999	7.51	strike slip	1.38	4.83	297
8	1.4782	2.9	Duzce_ Turkey	1999	7.14	strike slip	0	6.58	281.86
9	2.2514	0.8	Tottori_ Japan	2000	6.61	strike slip	28.81	28.82	293.37
10	2.6217	2.3	Sierra_ Mexico	2010	7.2	strike slip	18.21	19.47	242.05
11	2.8444	0.9	Darfield_ New Zealand	2010	7	strike slip	14.48	14.48	280.26

4. ANALYSES OF FRAMES

4.1. General

This chapter utilizes some of the seismic analysis methods shown in Figure 4.1 to investigate the collapse capacity of frames using SeismoStruct software.

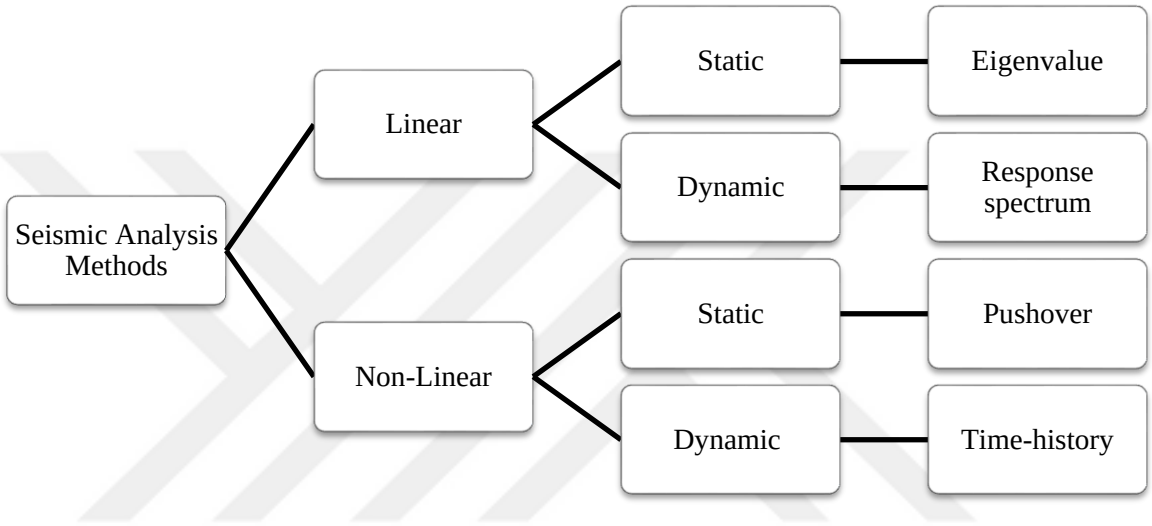

Figure 4.1. Seismic analysis methods

As will be described separately in the foregoing sections, three types of analyses were conducted which are linear static eigenvalue analyses, non-linear Static Pushover (SPO) analyses, and non-linear Incremental Dynamic Analyses (IDA).

The two-dimensional nonlinear models of the selected frames were prepared and static pushover analyses were conducted according to the mode shape obtained from eigenvalue analyses, either by ignoring and considering P-delta effects. The CCSM suggested by Adam and Jager (2012) was utilized to predict the "approximate collapse capacity" of the models. After computing these approximate results, incremental dynamic analyses (IDA) were carried out by using the matched ground motions. The collapse capacities obtained from these analyses for each frame were considered as 'exact' for the further stages of the study. The collapse capacities obtained from the approximate analyses using equivalent SDOF systems were then compared with the corresponding 'exact' values. This was conducted to check the convenience of available simplified methods to obtain the collapse capacity of buildings (CCSM proposed by Adam and Jager (2012)). The response of a non-ductile reinforced concrete (RC) frame

with/without OGS is assessed at the collapse prevention (CP) performance level in the light of various seismic code definitions. This is attempted by the evaluation of inelastic demands at the ground and first stories that are obtained from the nonlinear pushover and incremental dynamic analyses (IDA) of the numerical models.

4.2. Eigenvalue Analyses

The usual first step in performing a nonlinear static pushover analysis is determining the natural frequencies and mode shapes of the structure. These results characterize the basic dynamic behavior of the structural system. The eigenvalue analyses of the frame models were conducted and the dynamic properties of the selected frame at its fundamental mode of vibration are shown in Table 4.1. Besides, the mode shape vector, $\{\Phi\}$ that are illustrated in Figures 4.2 and 4.3 were obtained corresponding to the fundamental mode of both models. The generalized mass (M_1), well-known modal properties (L_1 and Γ_1), and base shear effective modal mass (M_1*) are calculated for the fundamental mode by using Eqs. (4.1)-(4.4). Here, m_j is the mass and Φ_{j1} is the modal displacement of the "j"th story at the fundamental mode.

$$M_1 = \sum_{j=1}^{N=5} m_j \times \phi_{j1}^2 \tag{4.1}$$

$$L_1 = \sum_{j=1}^{N=5} m_j \times \phi_{j1} \tag{4.2}$$

$$\Gamma_1 = L_1 / M_1 \tag{4.3}$$

$$M_1^* = \Gamma_1 \times L_1 \tag{4.4}$$

Table 4.1. Dynamic properties of the selected frame models

FRAME	M_1^* (t)	Fundamental Period T1 (s)	Γ_1	M_1 (t)	L_1 (t)
BF	98.94	1.133	1.288	59.666	76.832
OGS	138.10	0.709	1.111	111.9306	124.3272

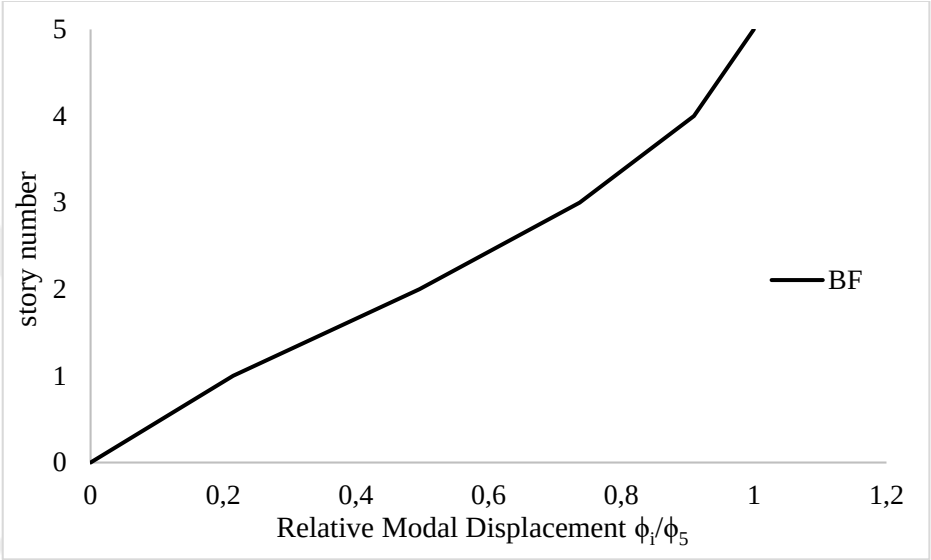

Figure 4.2. Mode shape for BF

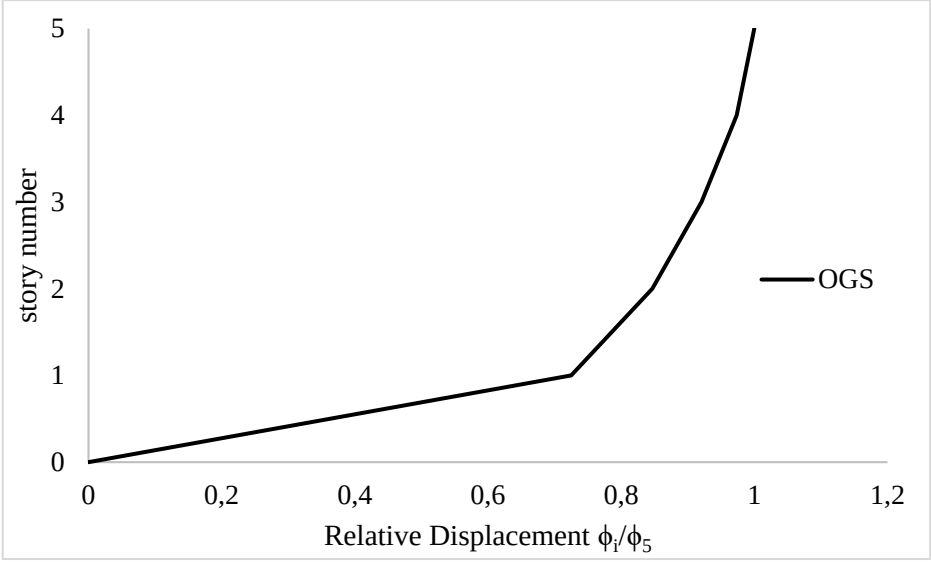

Figure 4.3. Mode shape for OGS

4.3. Non-Linear Static Pushover (SPO) Analyses

Once the modal properties of the selected frame models were determined by eigenvalue analyses, the nonlinear pushover analyses of models were carried out by utilizing Seismostruct software according to the mode shape obtained from eigenvalue analyses, either by ignoring and considering P-delta effects. At each story level, the nominal lateral loads are distributed to the nodes in accordance with the masses of these nodes. The P-delta effects are considered as the effects of geometrical non-linearities on the stiffness matrix by the employment of a total co-rotational formulation suggested by Correia and Virtuoso (2006). According to the manual of SeismoStruct, this formulation is based on «an exact description of kinematic transformations associated with large displacements».

Firstly, the pushover capacity curves of the models that were presented in Figures 4.4 and 4.5 were used to assess the critical structural members (i.e. columns) at the ground and first story according to the Turkish Earthquake Code (TEC, 2018). The design spectrum that is shown in Figure 4.6 was used to estimate the target displacement. This design spectrum is obtained for the location of the building that the frame belongs to according to the previous version of the TEC (2018). It should be noted that this previous version of the earthquake code is used since it was the formal code when this study was initiated. The design spectrum corresponds to a 10% probability of exceedance in 50 years and a 5% damping ratio. The lower and upper limit corner periods of the constant acceleration zone of the design spectrum are T_A=0.10 s. and T_B=0.48 s., respectively. The pushover capacity curves which are in base shear, V_b vs. roof drift, δ_{roof} domain are converted into the same spectral coordinates (spectral acceleration, S_a vs. spectral displacement, S_d) of the design spectrum (Figure 4.6) by using Eqs. (4.5) and (4.6). Φ_{N1} is the modal displacement of the roof level at the fundamental mode of vibration. (i.e. j=N).

$$S_a = V_b / M_1^* \tag{4.5}$$

$$S_d = \delta_{roof} / (\phi_{N1} \times \Gamma_1) \tag{4.6}$$

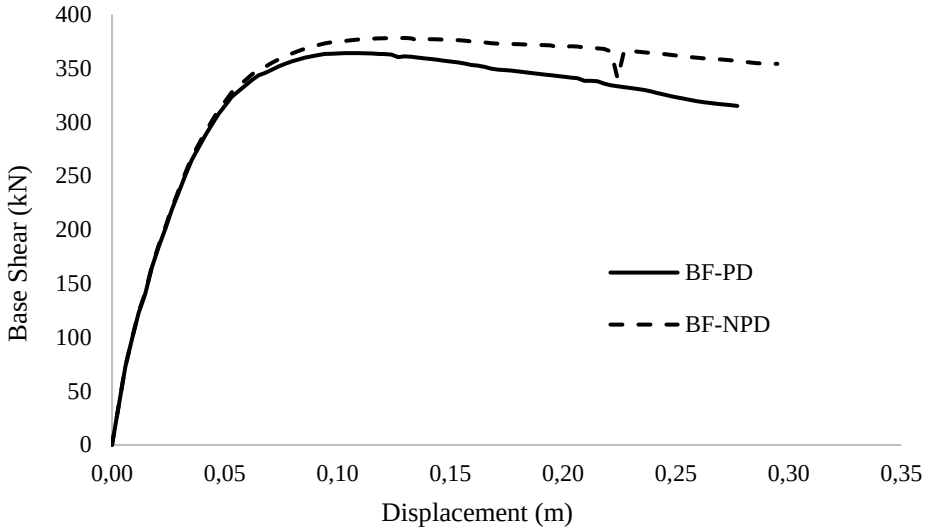

Figure 4.4. Pushover capacity curves of five story BF with and without considering P-Delta

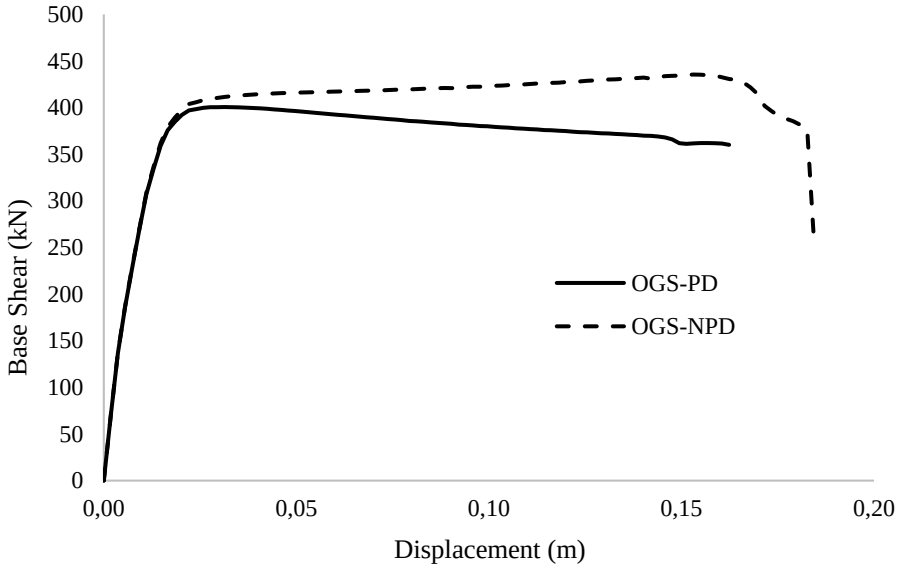

Figure 4.5. Pushover capacity curves of five story OGS with and without considering P-Delta

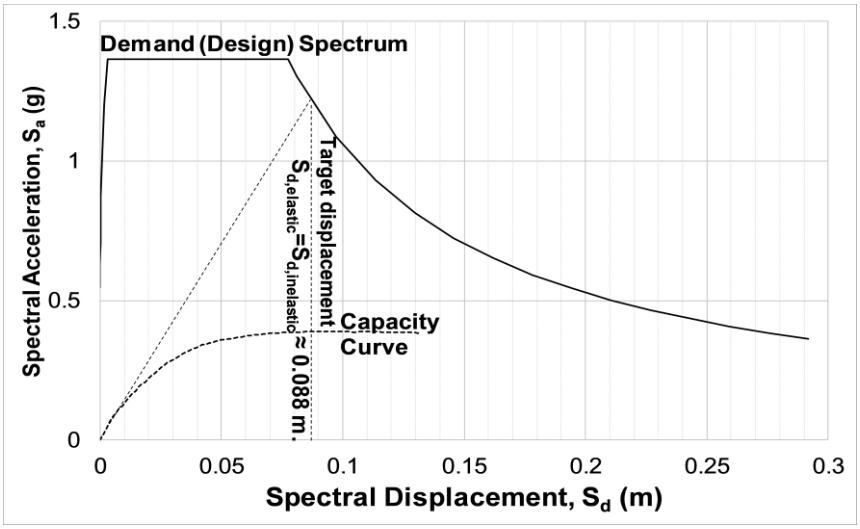

Figure 4.6. Determination of the target displacement for the BF model

In case of all models, the natural vibration periods (T_1) are larger than the upper limit corner period of the design spectrum (T_B) which enables the utilization of equal displacement approach (inelastic displacement demands, $S_{d,inelastic}$ are assumed as equal to the elastic displacement demands, $S_{d,elastic}$). The illustrative description of the target displacement determination procedure that is following the regulations of the TEC (2018) is shown in Figure 4.6 for the BF model. By inverted use of Eq. (4.6), these spectral target displacements were converted back into roof target displacements which are 0.113 m. and 0.078 m. for the BF and OGS models, respectively. The pushover analyses were repeated up to these roof target displacements to obtain the corresponding inelastic demand parameters, such as concrete strain and chord rotation of the columns.

4.3.1. Collapse Capacity Spectrum Method (CCSM)

The pushover capacity curves shown in Figures 4.7 and 4.8 were bi-linearized according to FEMA-356 (ASCE, 2000) in order to be used for the capacity spectum method. The global hardening ratio (α_s), elastic and inelastic stability coefficients (θ_e and θ_i), base shear and displacement corresponding to idealized yield point (V_y and X_{Ny}) were obtained from the bi-linear capacity curves in accordance with Adam and Jager (2012). These properties of the idealized pushover curve are illustrated in Figure 4.9.

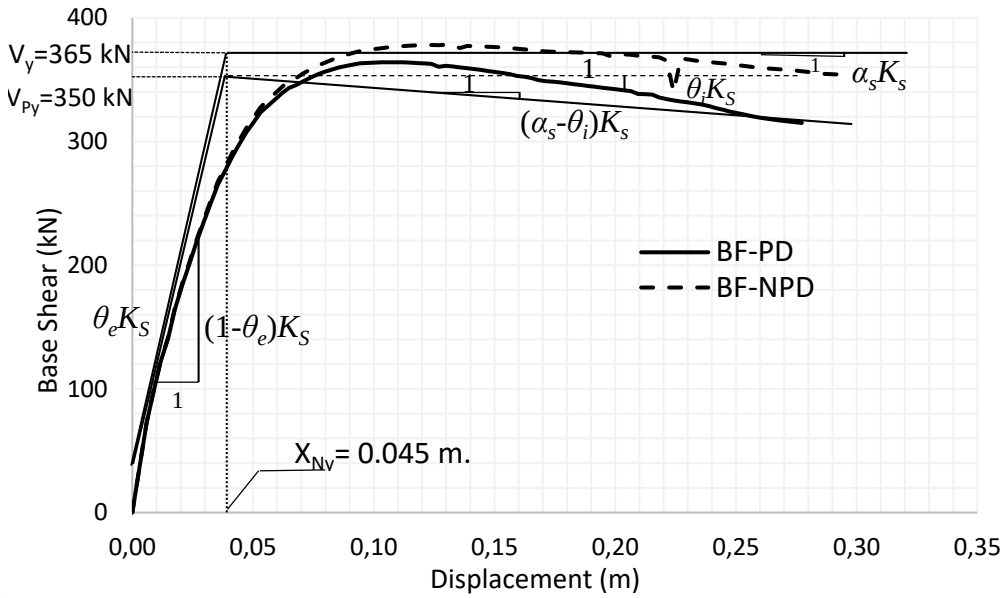

Figure 4.7. Idealization of pushover curves with and without considering P-Delta of BF structure

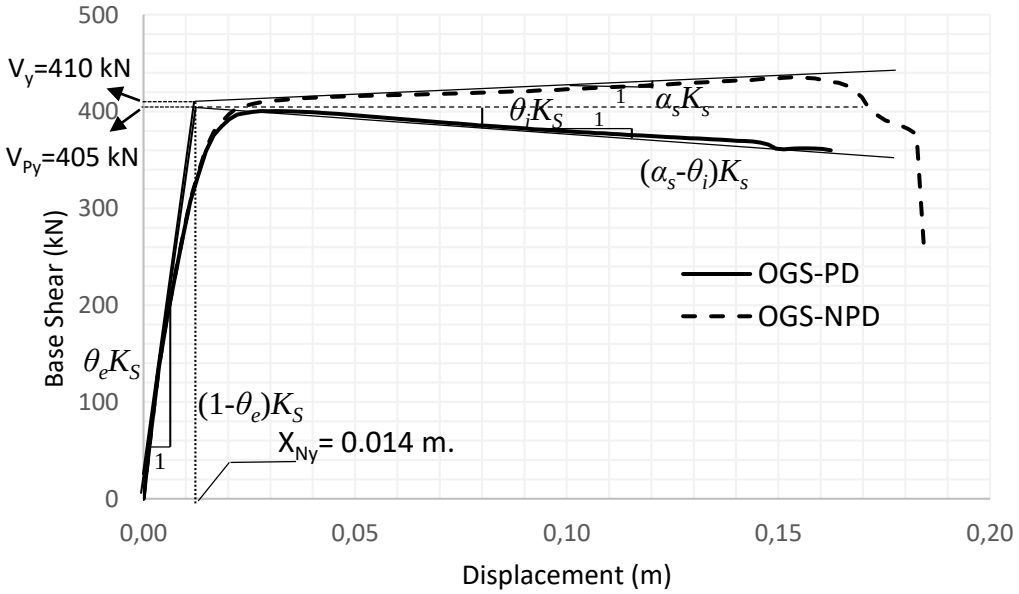

Figure 4.8. Idealization of pushover curves with and without considering P-Delta of OGS structure

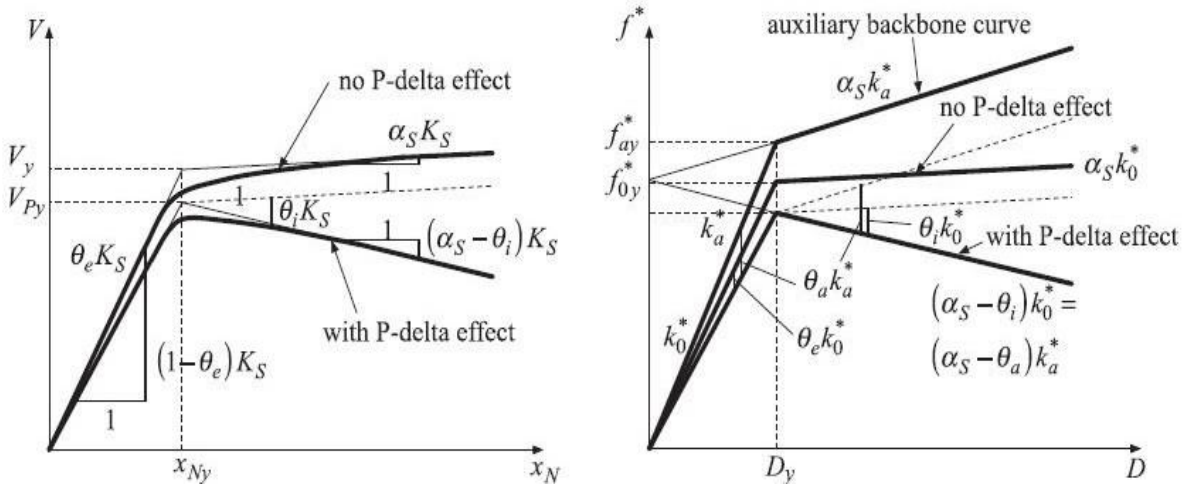

Figure 4.9. Illustration of the required parameters of the CCSM according to Adam and Jager (2012)

The essential parameters of the equivalent single degree of freedom ESDOF system required for the application of the collapse capacity spectrum methodology are the period T_a of the auxiliary ESDOF system, the auxiliary stability coefficient θ_a. These parameters are derived by Eqs. (4.7) -(4.9), respectively. According to Adam and Jager (2012):

$$T_a = 2\pi \sqrt{\frac{1-a_s}{v}} \sqrt{\frac{x_{Ny}}{V_y}} \sqrt{\sum_{i=1}^{N} \phi_i m_i} \tag{4.7}$$

$$\theta_a = \frac{\theta_i - \theta_e a_s}{v} \tag{4.8}$$

at which

$$v = 1 - \theta_e + \theta_a - a_s \tag{4.9}$$

where

X_{NY}: Roof displacement at onset of yield of the global pushover curve

m_i: Mass of the «i»th story

N: Number of stories

ϕ_i: «i»th Story element of the mode shape vector for the fundemantal mode

The viscous damping ratio was assumed as 5% and the collapse capacity (CC_d) was estimated by using Eqs. (4.10)-(4.12) that had been suggested by Adam and Jager (2012) for the CCSM. This collapse capacity was converted from the SDOF domain into the domain of the ESDOF system using coefficient λ_{MDOF} provided in Eq. (4.13). And finally, this value was assumed to be equal to the collapse capacity of the actual multi-degree of freedom (MDF) system (CC_{MDOF}=CC_{ESDOF}) Eq. (4.14).

$$CC_b = (T, \theta - \alpha) = \begin{cases} qT^p & T \le T_r \\ qT_r^p + qpT_r^{(p-1)}(T - T_r) & T > T_r \end{cases} \tag{4.10}$$

with

$$q(\theta - a) = \frac{2}{3}(\theta - a)^{-2/3}, p(\theta - a) = \frac{3}{100}(\theta - a)^{-7/10} + \frac{1}{10} \tag{4.11}$$

$$T_r = (\theta - \alpha) = \begin{cases} 40(\theta - \alpha) - \frac{2}{5} & (\theta - \alpha) \le 0.10 \\ \frac{18}{5} & (\theta - \alpha) > 0.10 \end{cases} \tag{4.12}$$

$$\lambda_{MDOF} = \left(\sum_{i=1}^{N} \phi_i m_i\right)^2 / \left(\sum_{i=1}^{N} m_i \sum_{i=1}^{N} {\phi_i}^2 m_i\right) \tag{4.13}$$

$$CC_{ESDOF} = \frac{CC_b}{\lambda_{MDOF}} \tag{4.14}$$

The method used to obtain the properties of idealized pushover curves is presented in Figure 4.10. And the properties of idealized pushover curves and properties of the equivalent SDOF systems utilized for the collapse capacity spectrum methodology are summarized in Tables 4.2 and 4.3, respectively.

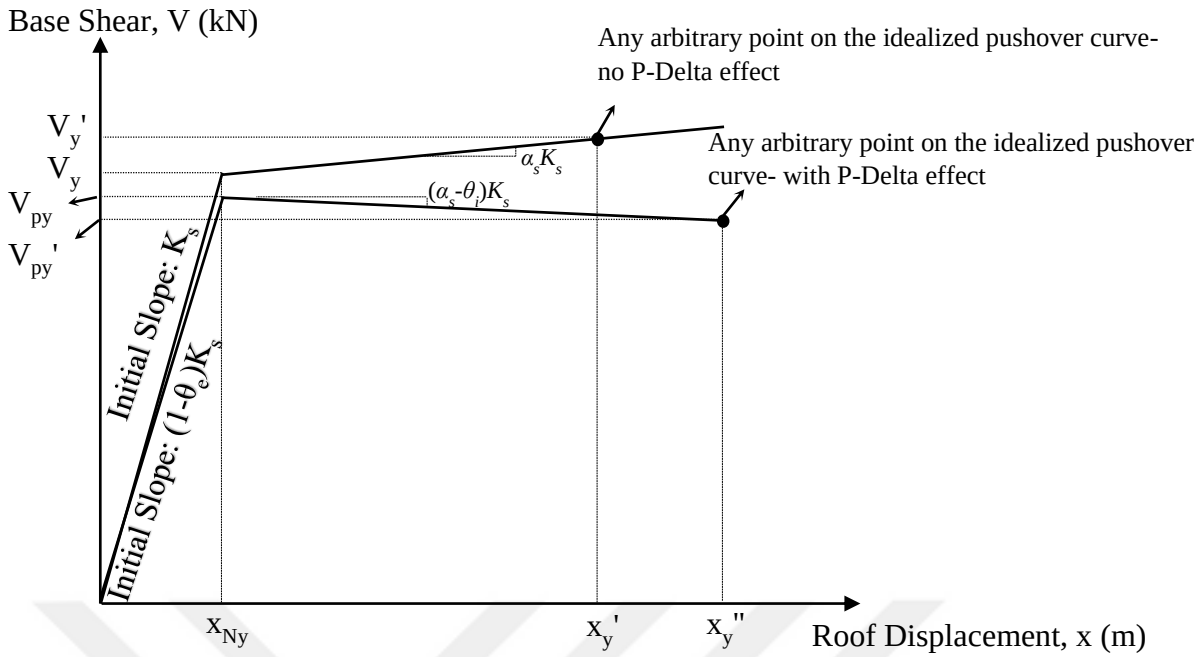

Figure 4.10. Applied method for idealized pushover curves properties

Table 4.2. Properties of idealized pushover curves

Frame	NPD Yield Base Shear Force V_y (kN)	Yield Roof Displacement X_{Ny} (m)	V_y' (kN)	X_y' (m)	PD Yield Base Shear Force V_{Py} (kN)	V_{py}' (kN)	x_y''(m)
NPD-BF	365	0.045	365	0.296	350	315	0.277
PD-BF							
NPD-OGS	410	0.014	436	0.16	405	360	0.16
PD-OGS							

Table 4.3. Properties of the equivalent SDOF systems

Frame	Effective Stiffness Ks (kN/m)	Hardening Ratio a_s	Elastic Stability Coefficient θ_e	Inelastic Stability Coefficient θ_i	ν	θ_a	Post-yield Stiffness Ratio θ_a-a_s	Ta (s)	λ_{MDOF}
NPD-BF	8111.111	0.000	0.041	0.041	0.978	0.019	0.019	0.619	0.843
PD-BF									
NPD-OGS	29285.714	0.006	0.012	0.017	0.998	0.017	0.010	0.408	0.988
PD-OGS									

Median collapse capacities of five-story BF and OGS frame structures according to the collapse capacity spectrum methodology based on equivalent single-degree-of-freedom systems are shown in Table 4.4.

Table 4.4. Results from collapse capacity spectrum methodology

Frame	CC_b	CC_{ESDOF}
BF	7.32	8.69
OGS	9.35	9.47

These results will be compared with the 'exact' collapse capacities obtained from incremental dynamic analyses (IDA) which is explained in the next section.

4.4. Incremental Dynamic Analyses (IDA)

In order to evaluate the CCSM and assess seismic code limits for the collapse state (or near collapse), collapse capacities based on time history analyses of the frame models should be obtained. Therefore, the case study frames were analyzed using the selected ground motion records by utilizing Seismostruct software to represent the complex structural behavior under seismic excitations.

After completing the modeling of the two-dimensional frames, nonlinear time history analyses were carried out using eleven different ground motions presented in Table 3.2. These records were acquired from Pacific Earthquake Engineering Research Center (PEER) "NGA-West 2" database according to an earthquake scenario chosen for an arbitrary location in Aydın, Turkey. The parameters considered for the earthquake scenario are presented in Chapter 3. The selected ground motion records (Figure 4.11) were matched with the design spectrum that was obtained for the selected coordinates by utilizing SeismoMatch (2018). A two stages of matching were applied, first up to 1 sec., and then up to 4 sec. period, with a maximum misfit tolerance of 30 percent. The resulting matched spectrums are presented together with the design spectrum in Figure 4.12 which also indicates the fundamental periods of the models and upper limit corner period. The resulting matched ground acceleration records are presented in Appendix 1, were used for the incremental dynamic analyses. The incremental dynamic analyses (IDA) were conducted by using scaling factors between 0.1-1.3 with an increment of 0.2 at each step (7 steps). In other words, the structural models were subjected to the ground motion records which were scaled by multiplying with these factors. And the results are presented in terms of base shear (or related spectral acceleration) vs. maximum roof drift ratio (IDA envelope curves) for each earthquake record. The damage measure (selected as maximum roof drift ratio) and the intensity measure (selected as max.base shear) were obtained at each

step of the IDA. It should be noted that it was not possible to apply all scale factors up to 1.3 in all cases and the analyses should have to stop due to convergence problems in these cases. Yet, in all analyses, the number of steps that could be applied was enough for the evaluations considered in this study.

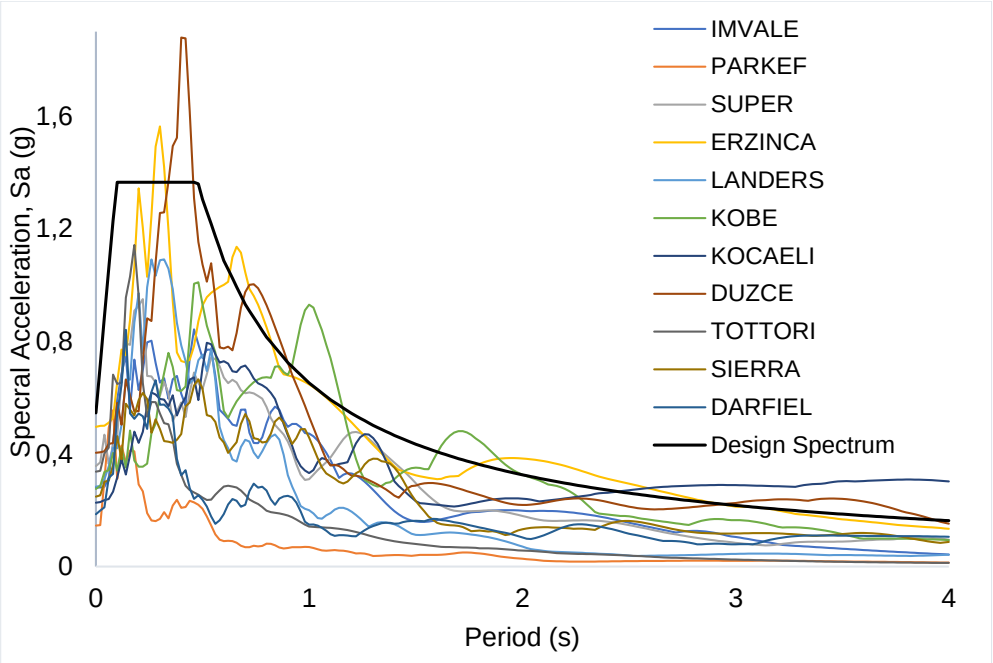

Figure 4.11. Pre-matched spectrums for the selected ground motions

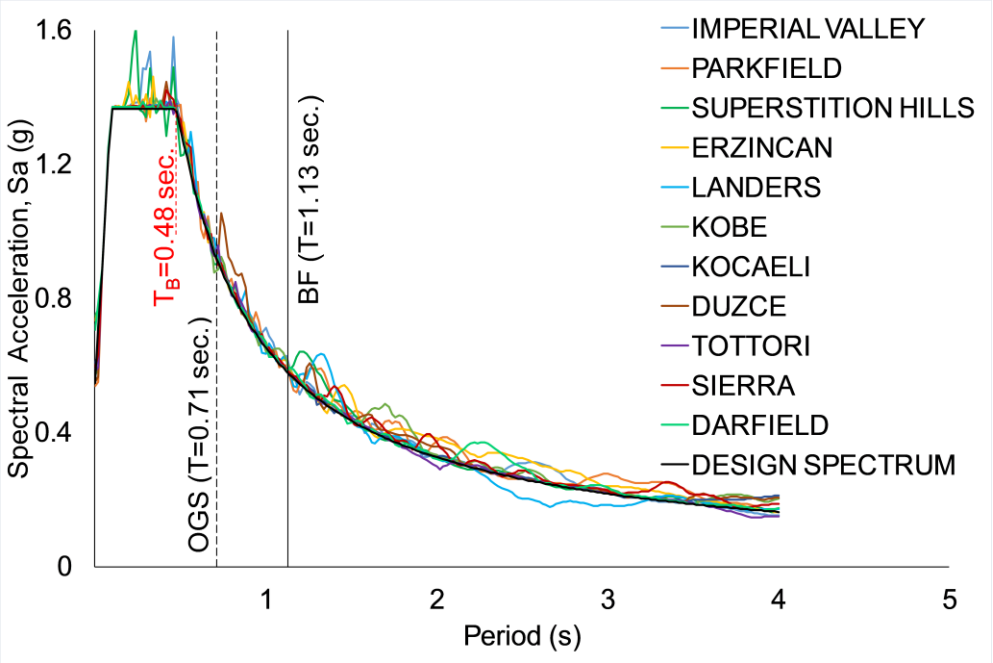

Figure 4.12. Post-matched spectrums for the selected ground motions

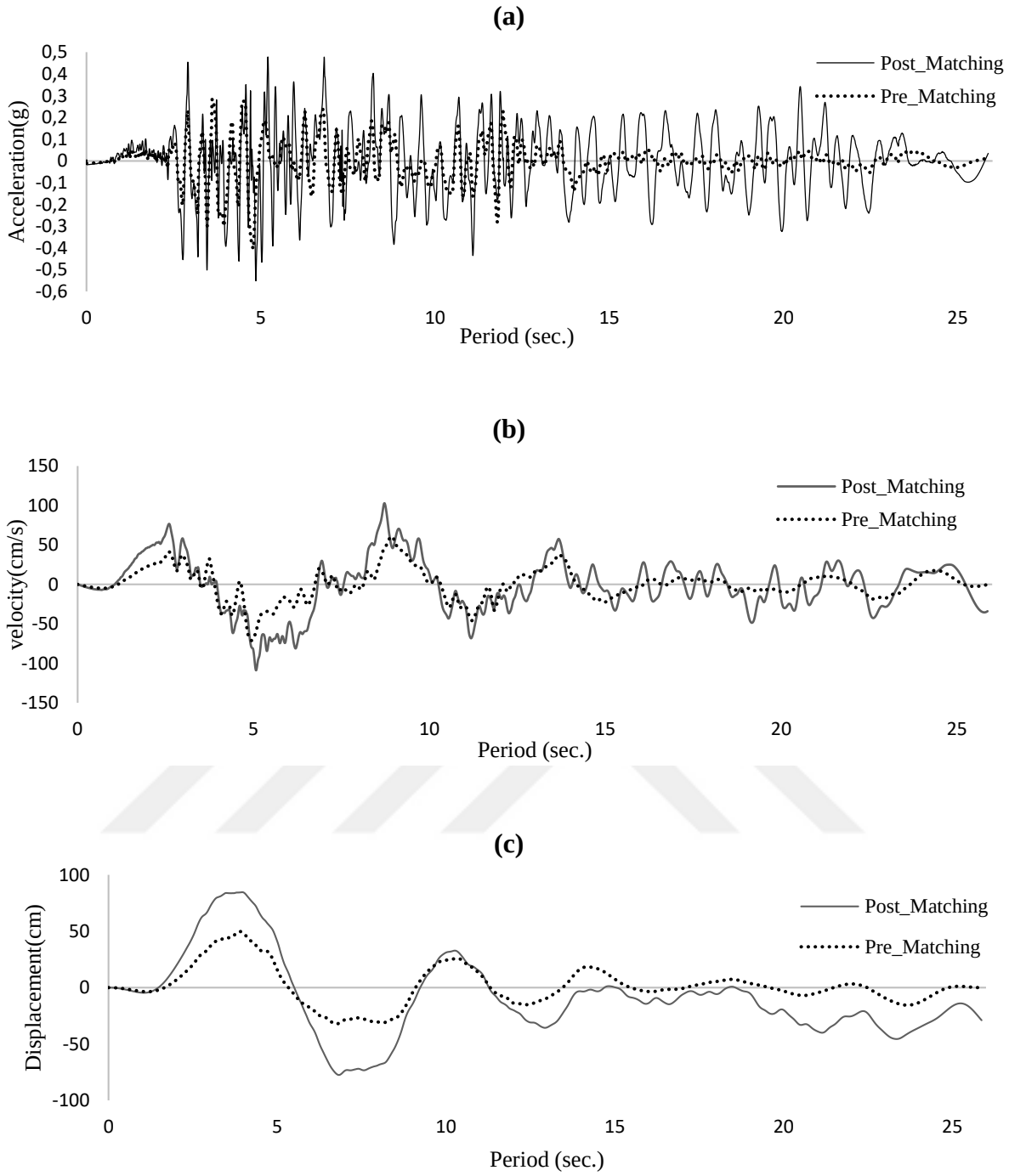

Figure 4.13. Pre and post matching for the selected ground motion Duzce (1999) different properties vs period (a) acceleration (b) velocity (c) displacement

5. RESULTS AND DISCUSSIONS

5.1. General

In this chapter, results obtained from both static pushover analyses (SPO) and incremental dynamic analyses (IDA) for a non-ductile RC bare frame and infilled frame with OGS with or without the consideration of the P-delta effect are evaluated. In Chapter 5.2, the collapse capacities obtained from IDA and CCSM are compared. In Chapter 5.3, the SPO and IDA results are evaluated with respect to the code limitations for the collapse state. And finally, the SPO and IDA results will be compared in different stages of the lateral response of the frames in Chapter 5.4.

5.2. Collapse Capacity

The actual collapse capacities of all models were obtained as a result of incremental dynamic analysis (IDA) where the models were analyzed dynamically by using successive ground motion records with increasing magnitudes (i.e. same record with increasing intensity of the ground motion record). Vamvatsikos and Cornell (2005) defines the base shear which is stabilized under increasing maximum drifts of the IDA curves as the collapse capacity of the structure. The graphical methodology that is utilized to obtain the collapse capacity is explained in Chapter 5.3.2.

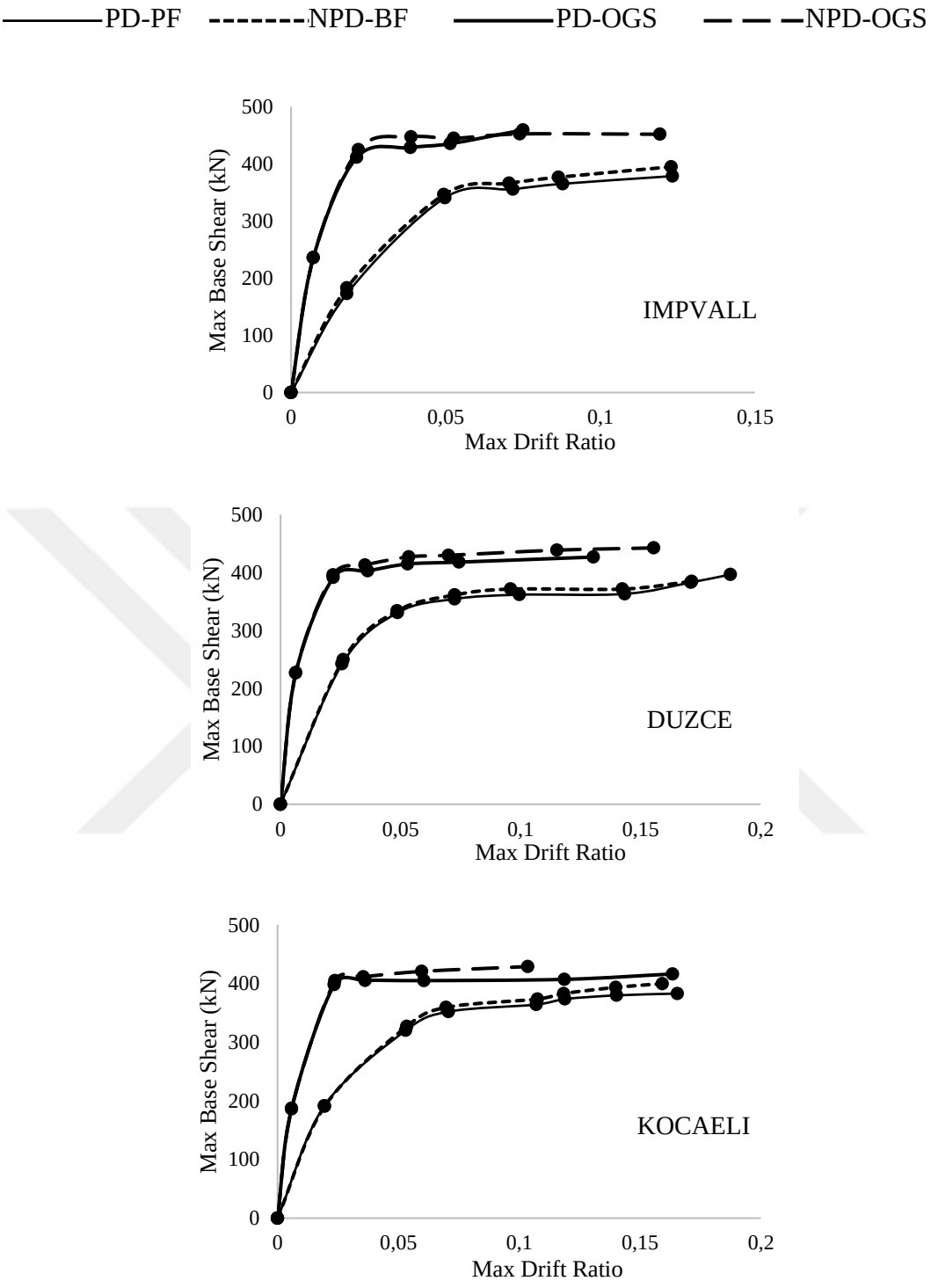

Figure 5.1. Base shear - drift ratio for the selected frame of 'IMPVALL','DUZCE' and 'KOCAELI' ground motions form IDA analyses

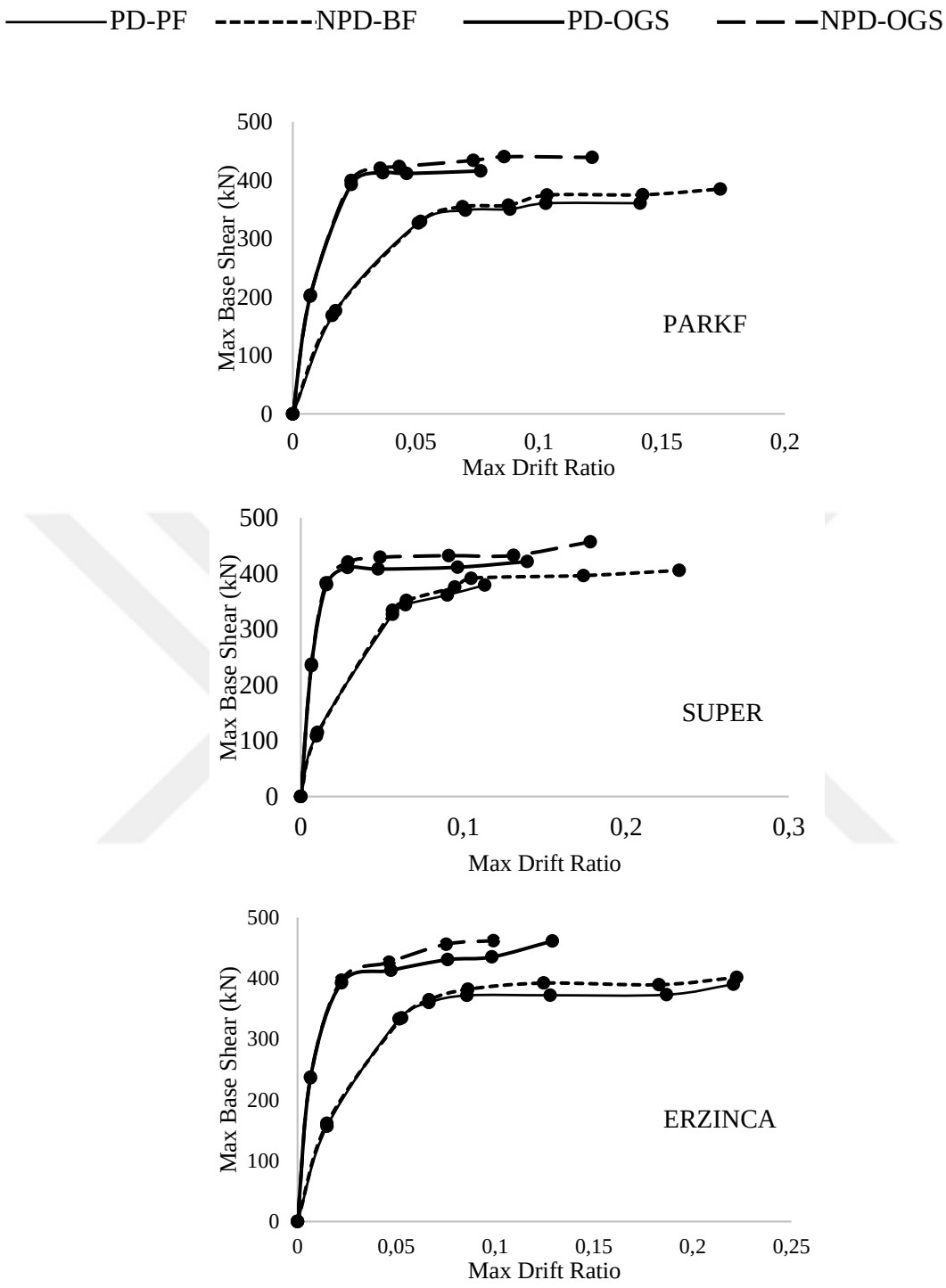

Figure 5.2. Base shear - drift ratio for the selected frame of ’PARKF’,’SUPER’ and ’ERZINCA’ ground motions form IDA analyses

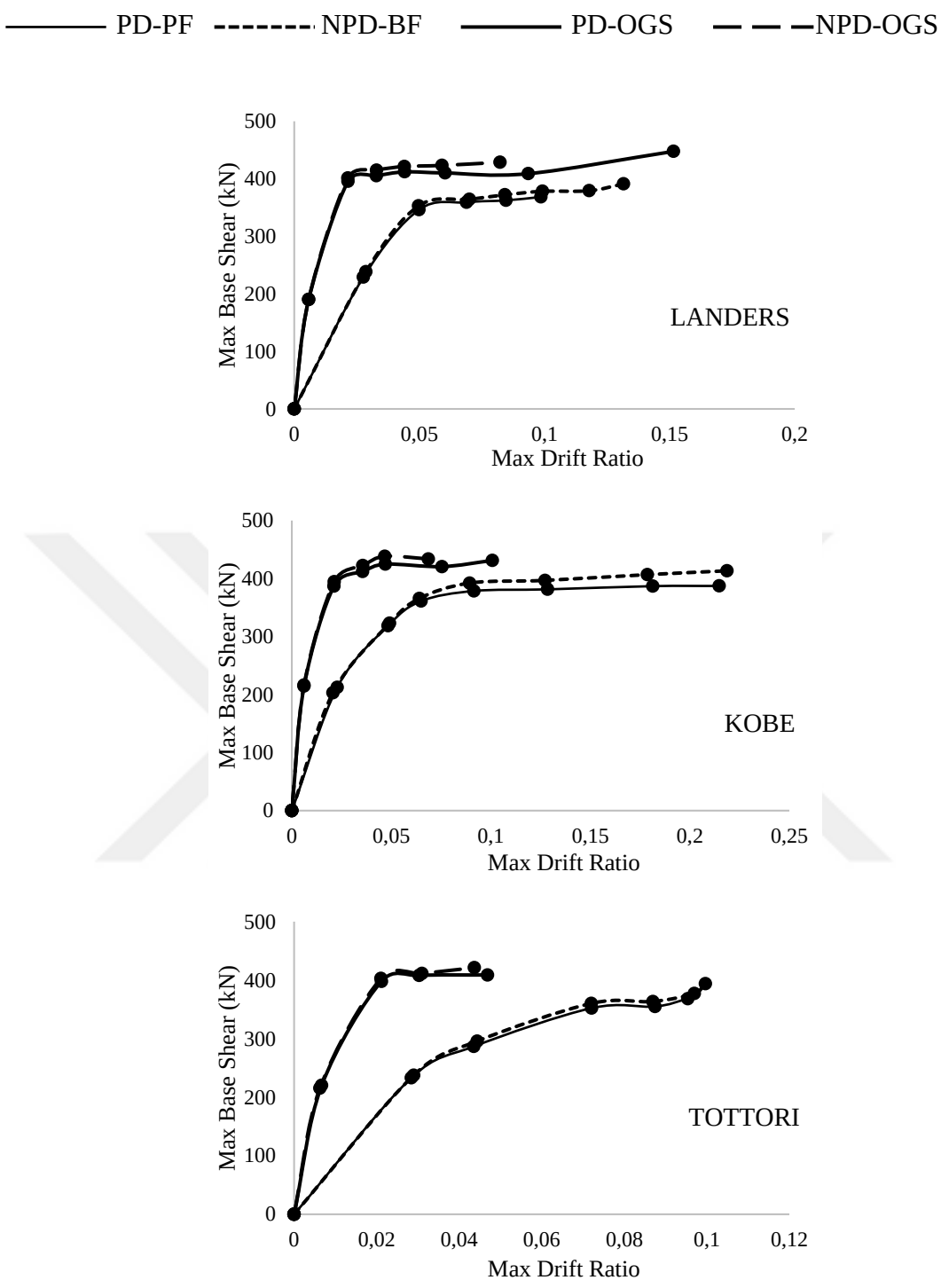

Figure 5.3. Base shear - drift ratio for the selected Frame of ’LANDERS’,’KOBE’ and ’TOTTORI’ ground motions form IDA analyses

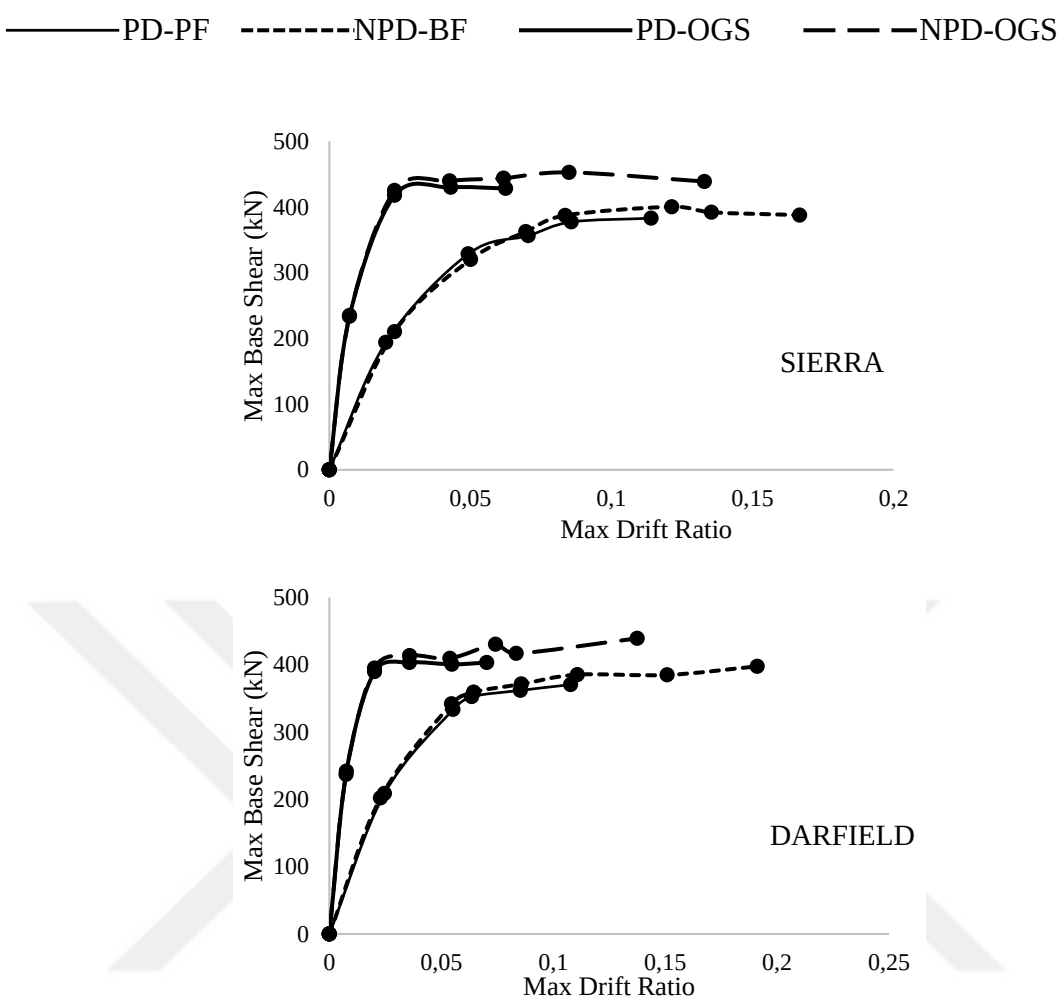

Figure 5.4. Base shear - drift ratio for the selected frame of ’SIRRA’ and ’DARFILD’ ground motions form IDA analyses

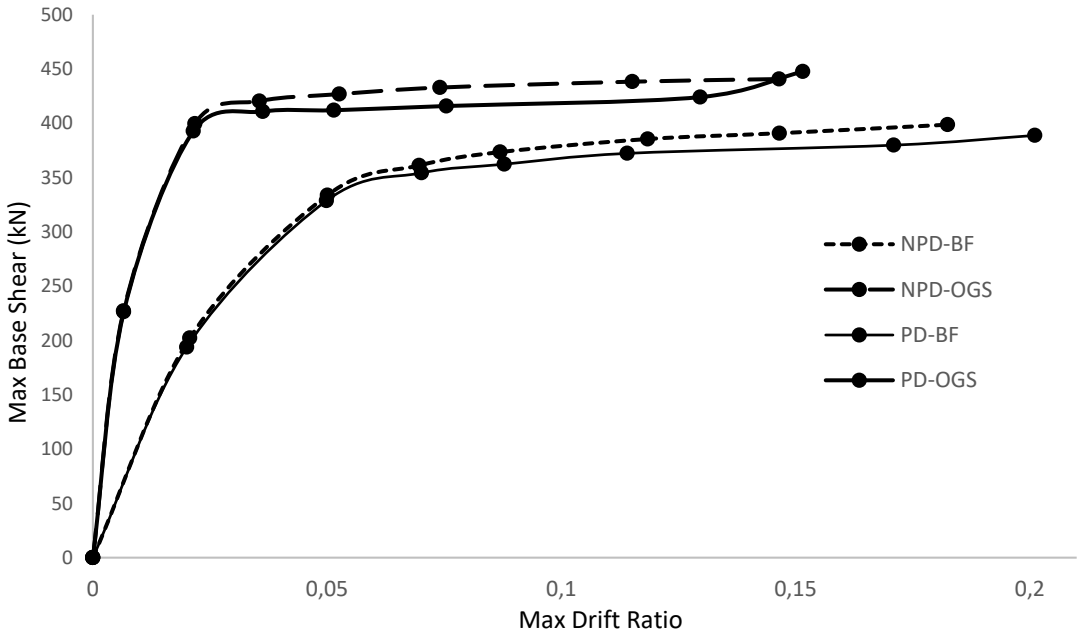

Figure 5.5. Median base shear - drift ratio for the selected frame form IDA analyses

In Figure 5.5 the median of all ground motions in terms of max base shear vs max draft ratio has been presented as a result of IDA analyses in both cases, with and without considering P-delta effects. The base shear has been converted to the spectral acceleration according to Eq. (5.1). The results obtained for the corresponding spectral accelerations were considered as the collapse capacity of the frames as shown in Table 5.1.

$$S_a = \frac{V}{M} \tag{5.1}$$

where

S_a: Spectral acceleration

V: Max base shear

M: Total mass

Table 5.1. Collapse capacities from IDA analyses

Frame	**Base Shear V (kN)**	**Total Mass M (t)**	**S_a**
BF	370	98.91	3.741
OGS	420	138.10	3.041

The collapse capacities obtained from the approximate CCSM and the mean values of those from IDA results are compared in Figure 5.6. It can be seen that the CCSM over-estimates the collapse capacity significantly when we compare the results of incremental dynamic analyses. Therefore, no further comparison has been done for this methodology.

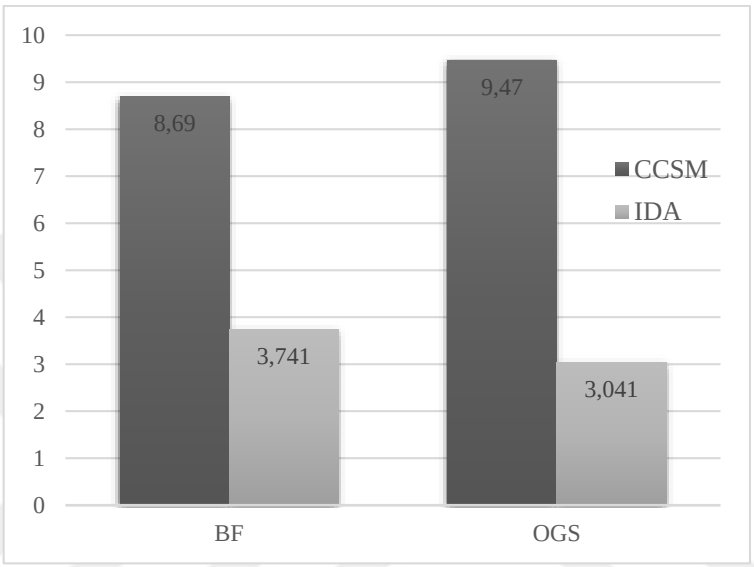

Figure 5.6. Collapse capacities of the BF and OGS models from the CCSM and IDA

5.3. Limit States

5.3.1. Results of Static Pushover Analyses

Figure 5.7 shows the pushover capacity curves and introduces the determined target roof drift for the BF and OGS models. When a comparison of BF and OGS models capacity curves is undertaken, it may be stated that the contribution of infill walls at the upper stories enhanced the initial rigidity which in return may change the base shear demand. Nevertheless, the comparison of the curves also shows that the infill walls of the OGS model could not provide an appreciable base shear capacity increase to counter the possible demand increment.

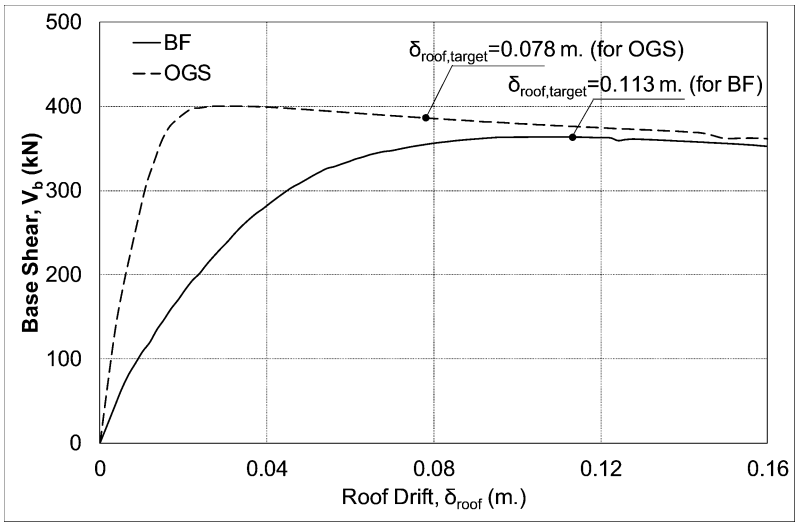

Figure 5.7. Pushover capacity curves of the BF and OGS models

An evaluation is undertaken for the possible accumulation of inelastic demand parameters, such as concrete strain, chord rotation and shear force in the columns due to OGS. The concrete strain values are only provided at the ground story. However, for comparison purposes the chord rotation and base shear demands at the first story level (i.e. above ground story) are also provided. These demand parameters are compared with the limiting values of Eurocode 8 (Eurocode 8, 2005) and TEC (2018) corresponding to varying damage states in Figure 5.8. In this figure, "SD" and "NC" represent "Significant Damage" and "Near Collapse" limit states according to Eurocode 8, respectively. In general, Eurocode 8 terminology is accepted although these limit states are termed as "Controlled Damage" and "Collapse Prevention" in the TEC (2018), respectively.

The calculation of the limit values of the codes is implemented using the details of the column section presented in Table 3.1 and the material properties provided in the previous sections. The calculations of the chord rotation capacities at the SD (0.0096 rad.) and NC (0.0128 rad.) limits, and shear force capacity at the NC limit (163.8 kN) were evaluated depending on sections A.3.2 and A.3.3 of the Eurocode 8, respectively. The concrete strain capacities at the SD (0.0051) and NC (0.0068) limit states were calculated according to section 5.8.1.1 of the TEC (2007). In these calculations, the columns were assumed as primary elements according to Eurocode 8. Therefore, the parameter used to define primary and secondary seismic elements (γ_{el}) was considered as 1.5 for the columns. The moment/shear ratio at the end section was assumed as half of the column height as suggested by TEC (2018). An average of the maximum axial loads at the ground story columns (i.e. 560 kN) as obtained from the time history analyses corresponding to the NC state defined by (FEMA350, 2000) was used. An

explanation is going to take a place in the next section for the determination of the NC limit state of FEMA 350 considering the IDA results. By ignoring the contribution of mid-reinforcement (2ϕ18) to the compressive or tensile resistance, the tension and compression reinforcements of the columns were assumed as 4ϕ18 (i.e. the reinforcements at either end of the section). Since there are no diagonal reinforcements in the section, the diagonal reinforcement ratio, ρ_d was taken as equal to zero. The confinement effectiveness factor (α) was defined similarly in both Eurocode 8 and TEC (2018) and the corresponding α value was estimated as 0.42. A reduction for the calculated capacities of Eurocode 8 was considered regarding the lack of detailing for earthquake resistance and the use of smooth longitudinal bars. As it is the case for most of the substandard buildings in Turkey, the longitudinal bars were assumed to be lapped at the end regions of the members while implementing these reductions. The lap length (l_o) was taken to be larger than 15 times the bar diameter (d_{bL}); however, no certain value is assigned to this unknown length in the calculations (i.e. min (40, l_o/d_{bL}) was assumed to be 40). While calculating the concrete strain capacities, the reductions due to the use of plain longitudinal bars and 90° hook ends of the stirrups were applied as suggested by the TEC (2018).

Figure 5.8(a) shows that one of the ground story columns (C2) of the BF model is at the SD limit with respect to the concrete strain classification of the TEC (2018). Besides, the column C3 is close to this limit. Although the target displacement of the OGS model is smaller in comparison to the one in the BF, the demand values of the ground story columns are larger at the target displacement of the OGS model. Two of the ground story columns (C2 and C3) exceed the NC state where the other column is beyond the SD state in the OGS model. According to the chord rotation classification of Eurocode 8, all the ground story columns and only one column at the first story are between the SD and NC limit states in the BF model (Figure 5.8(b)). In the OGS model, the chord rotation demands of the ground story columns raise considerably to exceed the NC limit state; whereas those of the first story columns are decreased substantially when compared with BF. There seems to be no significant change of shear forces at the ground story columns due to OGS (Figure 5.8(c)). As anticipated, there was a significant reduction in the column shear forces due to the action of infill walls at the upper story of the OGS model in comparison to BF. Overall, the assessment by the SPO analysis according to the local chord rotation definition of Eurocode 8 seems to be more conservative compared to the local strain definition of TEC (2018) which is especially more prominent in the case of BF.

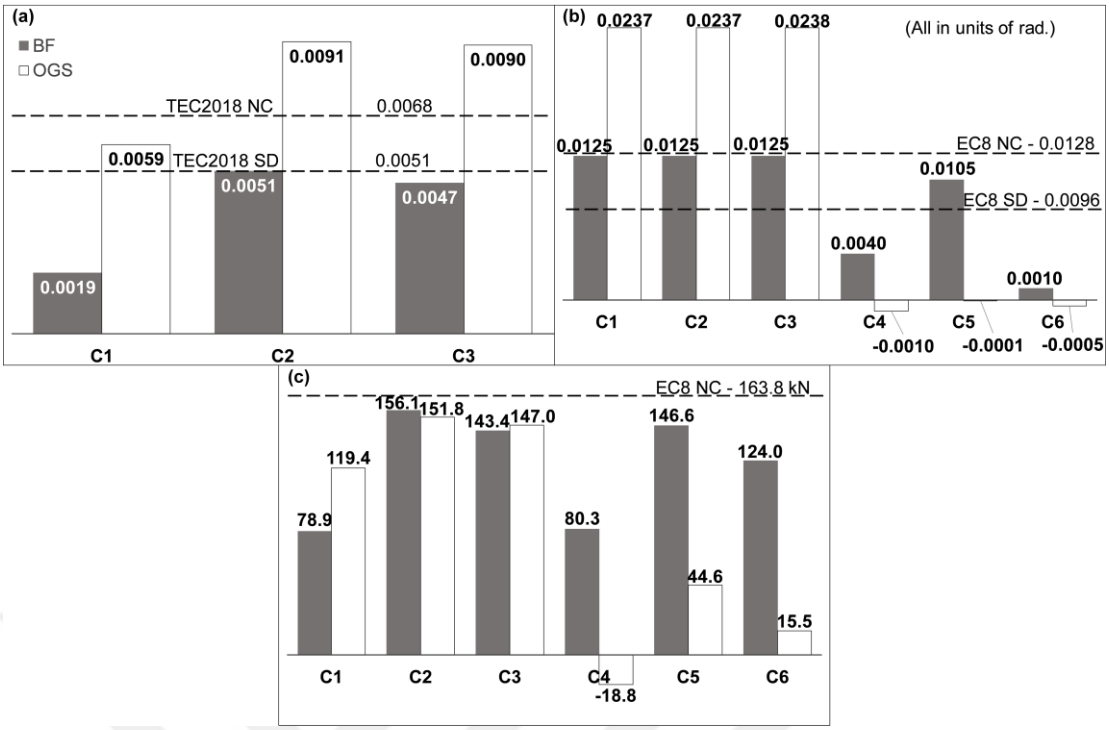

Figure 5.8. Pushover analyses results: (a) concrete strain at the ground story columns, (b) chord rotations and (c) shear forces at the ground and first story columns

5.3.2. Results of Incremental Dynamic Analyses

The intensity measure and engineering demand parameter of IDA curves were selected to be the base shear and roof drift, respectively to enable a comparison with the pushover results. The resulting IDA curves are shown in Figure 5.9(a) for all ground motion records and the statistical 16%, 50% (median), and 84% fractile curves are shown in Figure 5.9(b). When the global responses of BF and OGS models are compared statistically under raising intensities of different ground motion records, the dispersion is smaller for the BF model than it is for the OGS.

Vamvatsikos and Cornell (2005) defines the near-collapse (or collapse prevention) limit according to FEMA 350, either by a maximum inter-story drift ratio that reaches 10% for the steel moment-resisting frames or a point where the local slope of the IDA curve advances to 20% of the elastic slope. Since it depends on the graphical interpretation of the IDA curves, the definition corresponding to 80% lost in the elastic rigidity will also be utilized in this study for the NC limit state. Eurocode 8 has a definition for the chord rotation capacity of individual structural members at the NC limit state (i.e. 0.0128 rad. as given in Figure 5.8(b)). The TEC (2018) essentially defines the various limit states of damage depending on the concrete or

reinforcement strain capacities of each member. The concrete strain capacity of the columns at the NC limit state which is generally the more critical one for the existing structures with poor concrete quality is given in Figure 5.8(a) (i.e. 0.0068 mm/mm). It should be pointed out that except for the graphical interpretation suggested by Vamvatsikos and Cornell (2005), none of these limit state definitions consider the existence of infill walls in the structure. It is quite clear that any damage state defined according to graphical interpretation naturally accounts for all structural properties defined in the model, including the infill walls.

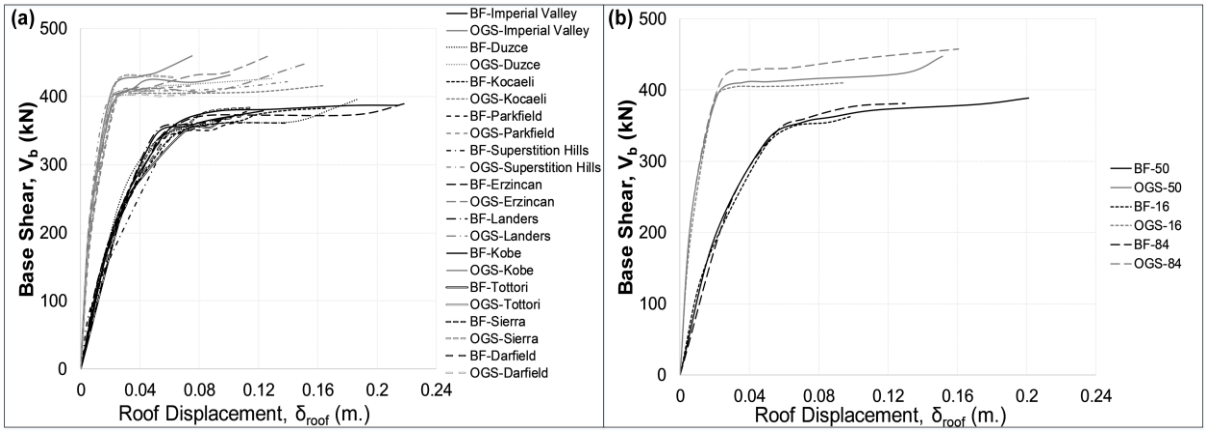

Figure 5.9. The IDA curves of BF and OGS models: (a) for all ground motion records, (b) 16%, 50% (median) and 84% fractile curves

Figure 5.10 illustrates the determination of the point where the slope of the tangent drops down to 20% of its initial elastic value for the median of all IDA curves. This is done for all BF and OGS models analyzed with each ground motion record. And the step of IDA that is closest to this point is defined as the NC limit state in each case. Consequently, the related engineering demand parameters, such as concrete strain and chord rotation are found at these steps of IDA. The median, 16th and 84th percentile of the concrete strain and chord rotation for the representative column "C1" (Figure 3.1) are illustrated in Figure 5.11 along with the corresponding NC limit state values defined by the codes.

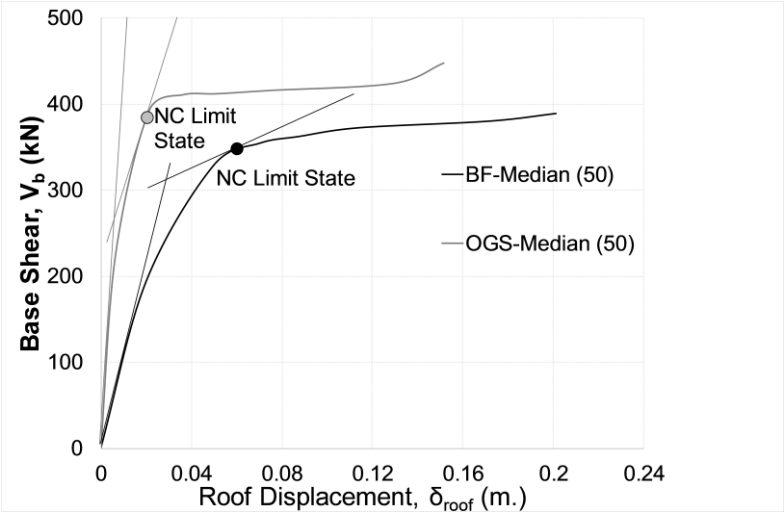

Figure 5.10. Determination of limit state for the near-collapse (NC) according to FEMA 350

As can be observed in Figure 5.10, the NC limit state corresponds to the transition region between the initial ascending portion and flat (or almost flat) second portion of the IDA curves for both BF and OGS. The NC is obtained at an earlier roof drift (i.e. with lower demand values) for the OGS model in comparison to BF. This may be related with two typical properties of the OGS model; first of all, the initial rigidity is larger and secondly, the transition from the initial ascending region to the flat second region is more abrupt in case of OGS compared to BF. This resulted in decreased engineering demand parameters in the OGS model corresponding to the defined NC limit state as illustrated in Figure 5.11 for column C2. Since their results are very close, the demand values of other ground story columns are not provided here.

In comparison to the graphical interpretation (FEMA350, 2000), the TEC (2018) appears to be more conservative in defining the NC limit state of the BF by utilizing the local strain in column C2 (Figure 5.11(a)). This conservatism ceases to exist in the OGS model where the NC limit is reached earlier according to FEMA 350. For column C2, the chord rotation limit according to the Eurocode 8 is substantially beyond the NC state determined by the graphical interpretation in both BF and OGS models. It should be emphasized once again that the same statements approximately apply for the other two ground story columns similarly.

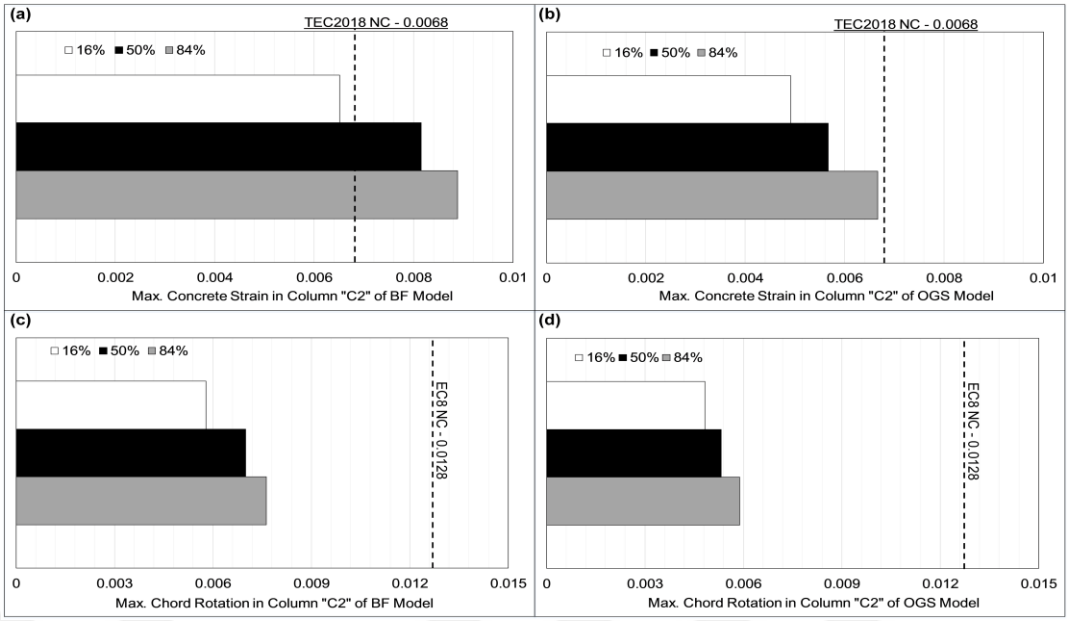

Figure 5.11. Maximum concrete strain and chord rotation at the NC limit state for column "C2"

The plastic hinge formations of all members were determined to evaluate the applicability of the NC limit state definition of FEMA 350 for the assessment of RC moment-resisting frames. This was carried out by checking the moment-rotation hysteretic curves of all frame members at the integration sections during the IDA step that was defined as the NC limit state. Figure 5.12 Shows the moment-rotation hysteretic curves of the bottom sections of columns C1 (ground story) and C4 (first story). In order to define the plastic hinge formation, an "idealized yield point" has been exceeded by column C1 bottom section (Figure 5.12(a)). Though, no inelastic response has been experienced by the bottom section of column C4. (Figure 5.12(b)).

Figure 5.13 shows the consequent plastic hinge distributions of the BF and OGS models at the IDA step related to the NC limit state of FEMA 350 and the next step for the Duzce record. The figure also illustrates the highest chord rotations observed on the ground story columns at these steps. As shown in Figure 5.13(a), collapse mechanism requirements are not fulfilled because the quantity of the plastic hinges is not enough to produce a collapse mechanism at the NC limit state of FEMA 350 for the BF at a chord rotation of 0.0074. Nevertheless, the collapse mechanism seems to be produced (not only at the ground but also at the first story level) in the next step when the maximum chord rotation was 0.0113 at the ground story. This indicates that the collapse takes place just after the NC limit state defined by FEMA 350. Therefore, the graphical interpretation of the NC limit state according to FEMA 350 definition may also be appropriate for the RC bare frames. On the other hand, the OGS model

has the potential to produce a collapse mechanism even at the NC limit state defined by FEMA 350. Accordingly, defining the NC limit state at an earlier stage may be considered as more suitable for the non-ductile RC frames with OGS.

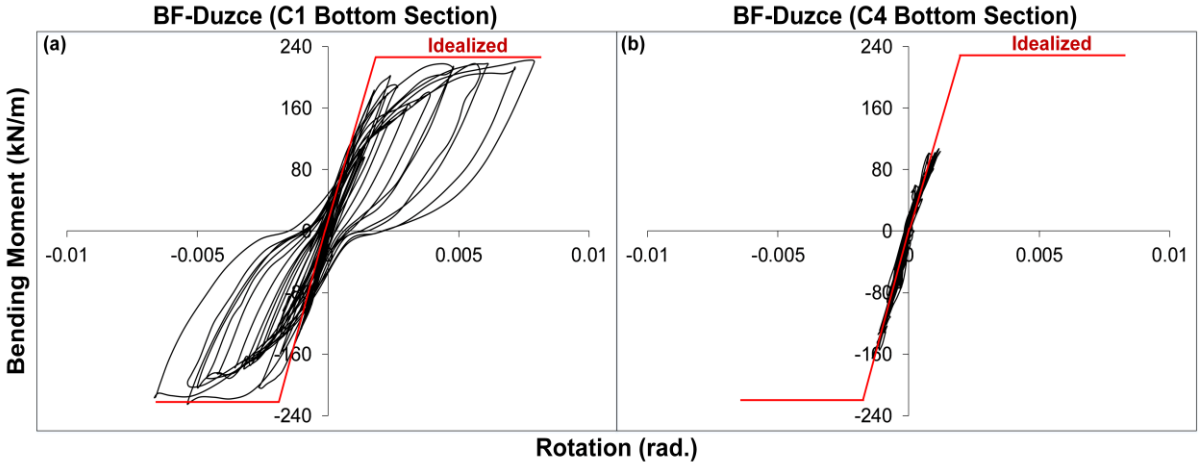

Figure 5.12. Moment-rotation hysteretic curves for the bottom sections of columns (a) C1 and (b) C4 at the NC limit state defined by FEMA 350

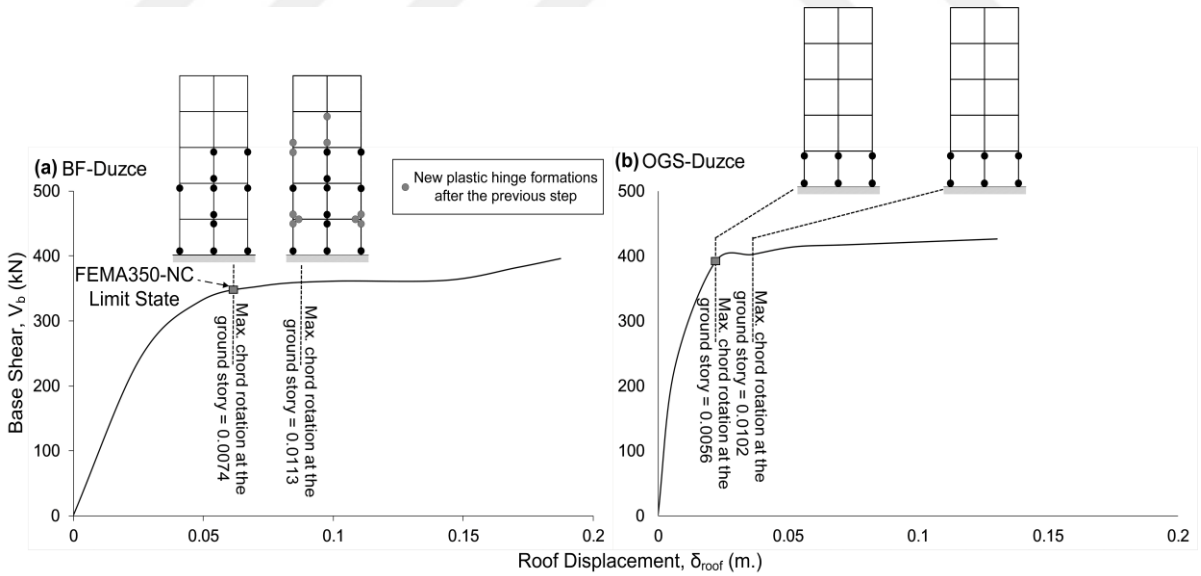

Figure 5.13. Distribution of plastic hinges in BF and OGS models at different steps of IDA under Duzce record

5.4. Comparison of SPO Analyses and IDA Results

Figure 5.14 illustrates the base shear vs. roof drift curves of SPO analyses and IDA (median) for the BF and OGS models. As demonstrated in this figure, the difference between SPO and IDA curves is nearly indistinguishable in the elastic region when the intensity measure and engineering demand parameters were chosen as the base shear and roof drift, respectively. This was also indicated by Vamvatsikos and Cornell (2005). However, as different from their results, the ultimate base shear (or spectral acceleration, S_a that can be determined by dividing base shear into the modal mass, M_1*) obtained by these two different analysis methods are also quite similar. The separation between the curves starts as the inelastic actions initiate, which is more considerable in the OGS model.

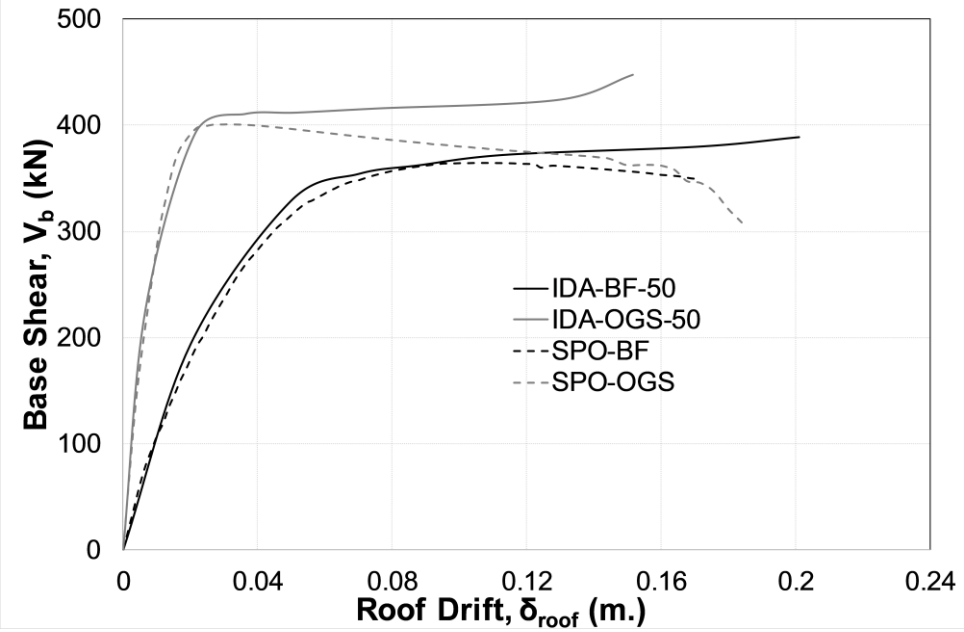

Figure 5.14. Base shear vs. roof drift curves of SPO analyses and median IDA

Figure 5.15 illustrates the comparison of the ultimate concrete strain and chord rotation of column C2 for three different stages on the SPO and IDA curves (i.e. using the Imperial Valley record for demonstration). In the case of BF, the local demand parameters also diverge along with the separation of the curves under the inelastic response, as demonstrated in Figure 5.15. It becomes evident in this figure that the local demand values which were not far from each other at the initial elastic response begin to differentiate for the SPO and IDA results during the inelastic response. This appears to be more substantial for the concrete strain in comparison to the chord rotation, which further explains more conservative assessment by the SPO analysis

in accordance to the chord rotation (i.e. concrete strain remains lower in the SPO). Despite the fact that the differentiation of SPO and IDA curves is more notable during the inelastic response of OGS, the inelastic demand values as a result of these two different analysis methods at the identical roof drift are very close even in the inelastic range. This may be a result to the accumulation of demand at the ground story in the OGS model. The scale of the distribution of damage in between the stories of BF which may be different for the SPO and IDA may cause the varying demand values in this model.

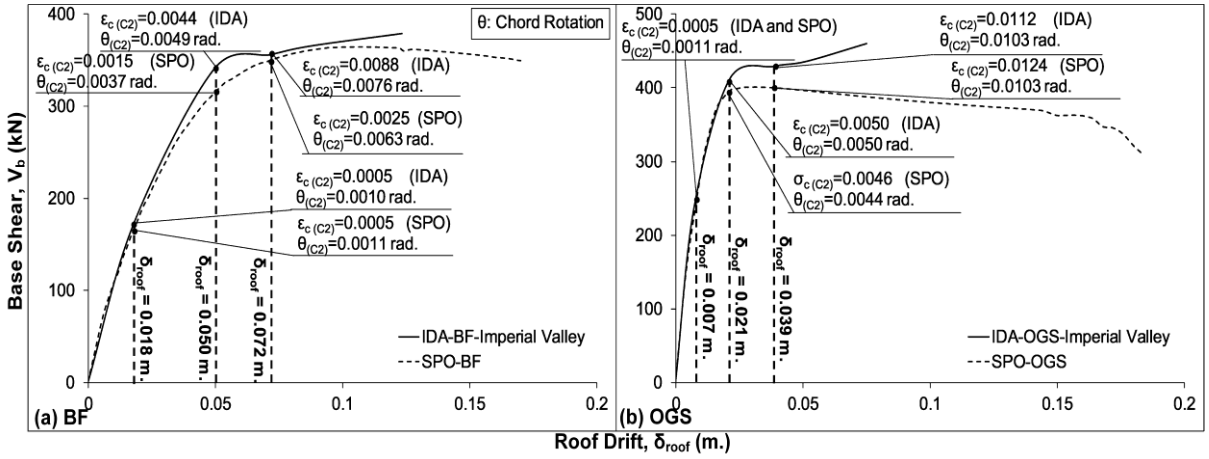

Figure 5.15. The local demand values of column C2 at different stages of the SPO and IDA curves: (a) for BF and (b) for OGS

6. CONCLUSIONS

6.1. Summary

In this study, the collapse capacity of regular non-ductile (RC) bare frame (BF) and brick infilled open ground story (OGS) frame structures which may be vulnerable to the global P-delta effect were evaluated using SPO and IDA analyses methods. Besides, the nonlinear seismic assessment of the models with respect to the damage limit states defined by different seismic codes was also conducted.

6.2. Conclusions

Based on the obtained results from the analysis of the non-ductile RC frame models, it can be concluded that:

- CCSM which considers P-Delta effects over-estimates the collapse capacity significantly in comparison with the results of IDA where P-Delta effects are taken into account. This may be related with the fact that CCSM is not based on the nonductile structures as considered in this study.
- Collapse capacity estimated by the CCSM for BF model was lower in comparison to the OGS frame. This is in contradiction with the other analyses results of this study. The collapse capacity of BF was larger than the one obtained for the OGS model as a result of IDA.
- Even though the target displacement of the BF was larger in comparison to the one in the OGS, the demand values were larger at the target displacement of the OGS model, as a result of the evaluation of SPO analyses.
- The shear demand at the ground story was very close in the BF and OGS models at the target displacement of the SPO analyses. As expected, the column shear forces were significantly reduced at the first story of OGS model compared to BF in the same analysis results.
- The results of SPO analyses showed that Eurocode 8 was more conservative in the assessment of the BF model employing the local chord rotation definition compared to the local concrete strain definition of TEC (2018).

- The near collapse limit state definition of FEMA 350 from the graphical interpretation of IDA results was assessed according to the sidesway mechanisms caused by the adequate plastic hinge formations on the model. As a result, it may be concluded that the FEMA 350 defined the collapse state of the nonductile RC frame model successfully, although it was originally generated for the steel frames.
- In the case of OGS model, the signs of collapse due to sidesway mechanism seem to take place at an earlier stage of IDA analyses compared to the near collapse limit state determined by the FEMA 350 approach. Therefore, a more suitable definition of near collapse limit state may be required for the frames with certain irregularities.
- Referring to IDA, the near-collapse limit state suggested by FEMA 350 corresponded to a much lower chord rotation compared to the one suggested by Eurocode 8 for the near-collapse limit state for both cases BF and OGS models. Therefore, FEMA 350 suggestion was more conservative than the Eurocode 8 suggestion. By considering the previous conclusions, the chord rotation limit of Eurocode 8 may be stated as unsafe especially for the nonductile OGS model considered in this study.
- Considering the IDA results, the TEC (2018) was more conservative in defining the NC limit state of the BF by utilizing the local concrete strain for the columns, unlike the outcome from the SPO analyses. This conservatism disappeared in the OGS model where the NC limit is reached earlier according to FEMA 350.
- The results indicate that the early collapse of nonductile OGS frames without producing noticeable inelastic actions should be considered in the limit state definitions of the seismic codes for the assessment of buildings.
- In general, the base shear vs. roof drift curves obtained by SPO analyses and IDA are close to each other for the BF model. The same conclusion was also valid for the local demand values obtained by these two analysis methods during the initial stage. However, the local demand values of BF obtained by these methods start to deviate from each other as the inelastic actions progress in the structure. The deviation of the SPO and IDA results was more significant in the case of concrete strain which had lower values in the SPO.
- Despite the differentiation of SPO and IDA curves during the inelastic response of OGS was more appreciable, the inelastic demand values of both analysis methods were convergent even in the inelastic range.

- The conclusions in this study should not be generalized without conducting further studies, where a satisfactory number of RC buildings with various number of stories and irregularities are considered.

REFERENCES

ACI Committee 318 (2008). *Building Code Requirements for Structural Concrete and Commentary*. ACI 318M-08, Reported by ACI Committee 318, Farmington Hills, MI.

Adam, C., Ibarra, L. F., & Krawinkler, H. (2004, August 1-6). *Evaluation of P-delta effects in non-deteriorating MDOF structures from equivalent SDOF systems*. Thirteenth World Conference on Earthquake Engineering, Vancouver BC, Canada.

Adam, C. and Jäger, C. (2012). Simplified collapse capacity assessment of earthquake excited regular frame structures vulnerable to P-delta. *Engineering Structures*, *44*, 159–173. https://doi.org/10.1016/j.engstruct.2012.05.036

Akın, E. (2019). Open ground story in properly designed reinforced concrete frame buildings with shear walls. *Structures*, *20*, 822–831. https://doi.org/10.1016/j.istruc.2019.07.003

ASCE-American Society of Civil Engineers. (2000). *Commentary for the seismic rehabilitation of buildings*. FEMA-356, Washington, DC.

Bernal, D. (1998). Instability of buildings during seismic response. *Engineering Structures*, *20*(4–6), 496–502. https://doi.org/10.1016/S0141-0296(97)00037-0

Correia, A. A., & Virtuoso, F. B. E. (2006). *Nonlinear analysis of space frames*. In C. A. Motasoares, J. A. C. Martins, H. C. Rodrigues, J. A. C. Ambrósio, C. A. B. Pina, C. M. Motasoares, E. B. R. Pereira, & J. Folgado (Eds.), Third European Conference on Computational Mechanics, pp. 107–107. Springer, Netherlands. https://doi.org/10.1007/1-4020-5370-3_107

Dolšek, M. and Fajfar, P. (2001). Soft storey effects in uniformly infilled reinforced concrete frames. *Journal of Earthquake Engineering*, *5*(01), 1–12. https://doi.org/10.1080/13632460109350383

Eurocode 8. (2005). *European Standard EN 1998-3:2005: Design of structures for earthquake resistance - Part 3: Assessment and retrofitting of buildings,* Com. Eur. Norm. Brussels.

FEMA-Federal Emergency Management Agency. (2000). *Recommended seismic design criteria for new steel moment-frame buildings*. FEMA-350, Washington, DC. https://doi.org/10.1017/CBO9781107415324.004

Ibarra, L. F. and Krawinkler, H. (2005). *Global collapse of frame structures under seismic excitations*. Pacific Earthquake Engineering Research Center Berkeley, CA.

Kadaş, K. (2006) Influence of idealized pushover curves on seismic response Master's thesis, Middle East Technical University Graduate School of Natural and Applied Science, Ankara, Turkey.

Negro, P. and Colombo, A. (1997). Irregularities induced by nonstructural masonry panels in framed buildings. *Engineering Structures, 19*(7), 576–585.

Republic of Turkey Prime Ministry Disaster and Emergency Management Authority. (2018). *Turkish Earthquake Code for Buildings*, Ankara, Turkey.

Republic of Turkey Prime Ministry Disaster and Emergency Management Authority. (2007). *Turkish Earthquake Code for Buildings*, Ankara, Turkey.

Research data was evaluated using Seismostruct 2020 (Seismosoft Ltd., Milan. Italy) package program. Retrieved from https://www.seismosoft.com/seismostruct-prod.

Research data was evaluated using Seismomatch 2018 (Seismosoft Ltd., Milan. Italy) package program. Retrieved from https://www.seismosoft.com/seismomatch-prod.

Vamvatsikos, D., & Cornell, C. A. (2005). Direct estimation of seismic demand and capacity of multidegree-of-freedom systems through incremental dynamic analysis of single degree of freedom approximation. *Journal of Structural Engineering, 131*(4), 589–599.

APPENDICES

APPENDIX 1

MATCHED TIME HISTORY RECORDS

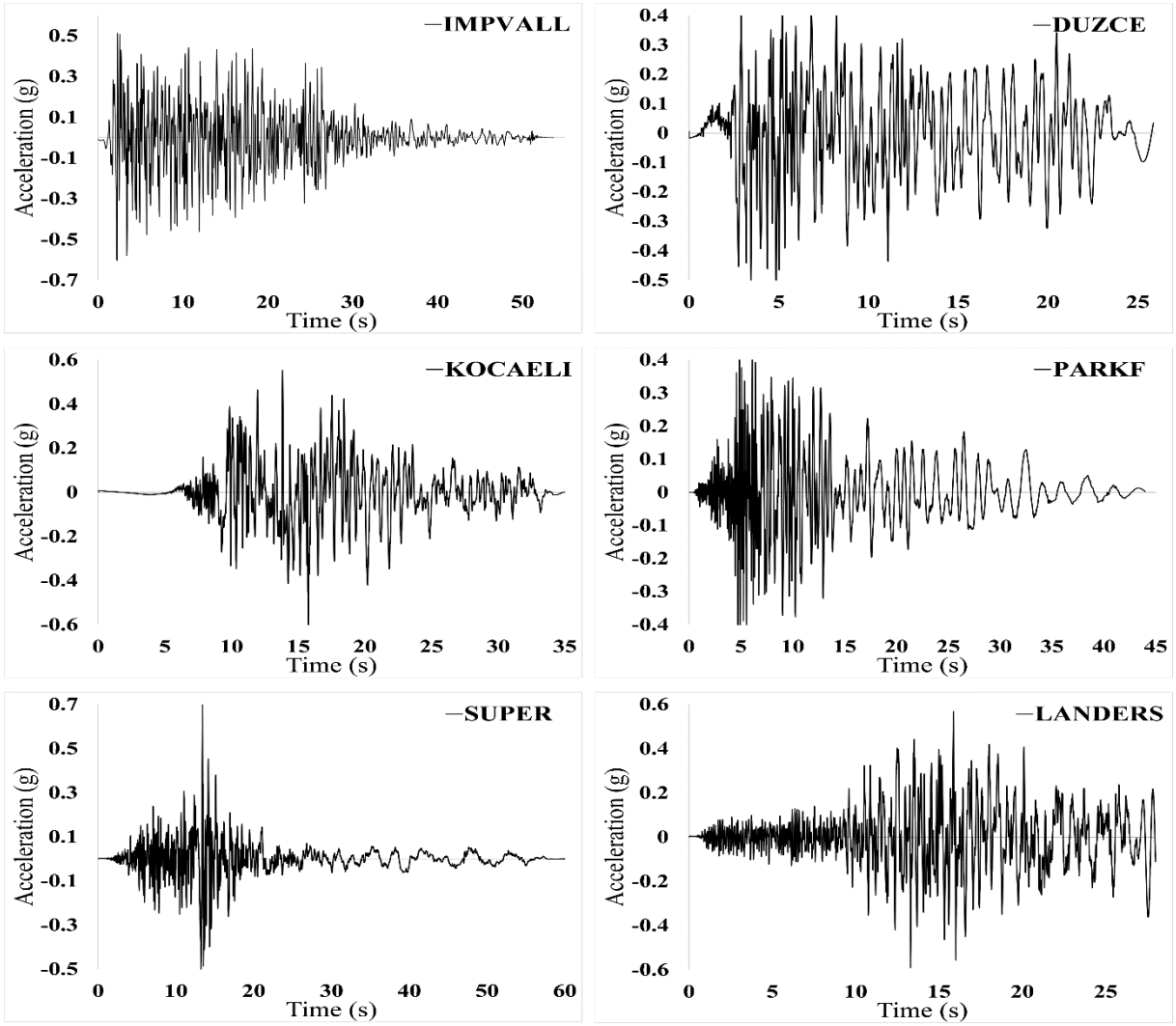

Figure Appendix 1. Matched ground motion records for the Imperial Valley (1940), Duzce (1999), Kocaeli (1999), Parkfield (1966), Superstition Hills (1987) and Landers (1992) earthquakes

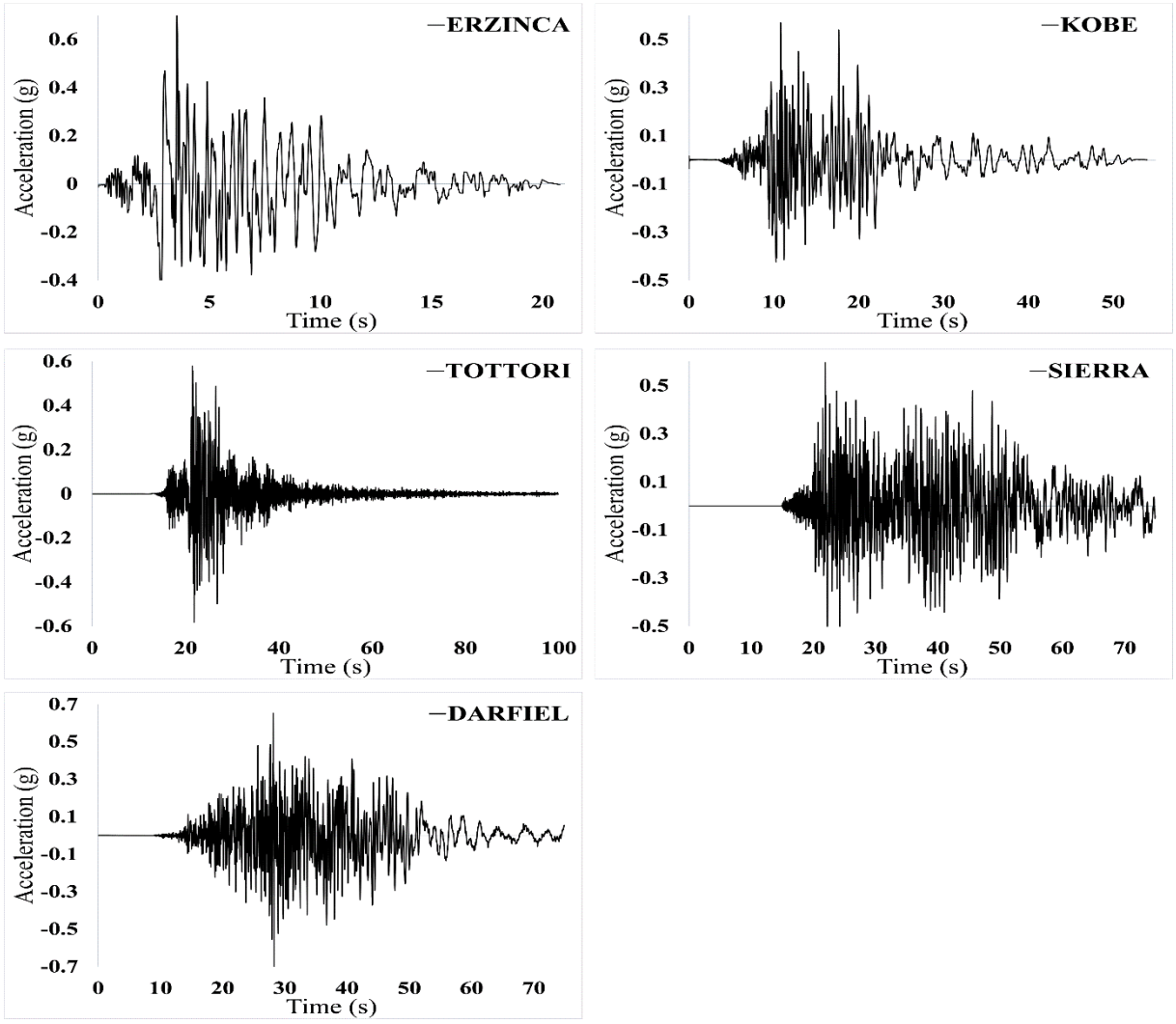

Figure Appendix 2. Matched ground motion records for Erzincan (1992), Kobe (1995), Tottori (2000), Sierra (2010) and Darfield (2010) earthquakes

T.C.

AYDIN ADNAN MENDERES UNİVERSITY

GRADUATE SCHOOL OF NATURAL AND APPLİED SCIENCES

SCIENTIFIC ETHICAL STATEMENT

I hereby declare that I composed all the information in my master's thesis entitled “SEISMIC COLLAPSE CAPACITY OF BRICK INFILLED REINFORCED CONCRETE FRAMES WITH OPEN GROUND STORY” within the framework of ethical behavior and academic rules, and that due references were provided and for all kinds of statements and information that do not belong to me in this study in accordance with the guide for writing the thesis. I declare that I accept all kinds of legal consequences when the opposite of what I have stated is revealed.

Emad KANAS

… / … / …